Molecular Therapy
Nucleic Acids
Original Article

Transient Retrovirus-Based CRISPR/Cas9 All-in-One Particles for Efficient, Targeted Gene Knockout

Yvonne Knopp,[1] Franziska K. Geis,[1] Dirk Heckl,[2] Stefan Horn,[3] Thomas Neumann,[1] Johannes Kuehle,[1] Janine Meyer,[1] Boris Fehse,[3] Christopher Baum,[1,4] Michael Morgan,[1] Johann Meyer,[1] Axel Schambach,[1,5] and Melanie Galla[1]

[1]Institute of Experimental Hematology, Hannover Medical School, Hannover 30625, Germany; [2]Pediatric Hematology and Oncology, Hannover Medical School, Hannover 30625, Germany; [3]Research Department Cell and Gene Therapy, Department of Stem Cell Transplantation, University Medical Center Hamburg-Eppendorf, Hamburg 20246, Germany; [4]Presidential Office, Hannover Medical School, Hannover 30625, Germany; [5]Division of Hematology/Oncology, Boston Children's Hospital, Harvard Medical School, Boston, MA 02115, USA

The recently discovered CRISPR/Cas9 system is widely used in basic research and is a useful tool for disease modeling and gene editing therapies. However, long-term expression of DNA-modifying enzymes can be associated with cytotoxicity and is particularly unwanted in clinical gene editing strategies. Because current transient expression methods may still suffer from cytotoxicity and/or low efficiency, we developed non-integrating retrovirus-based CRISPR/Cas9 all-in-one particles for targeted gene knockout. By redirecting the gammaretroviral packaging machinery, we transiently delivered *Streptococcus pyogenes Cas9* (*SpCas9*) mRNA and single-guide RNA transcripts into various (including primary) cell types. Spatiotemporal co-delivery of CRISPR/Cas9 components resulted in efficient disruption of a surrogate reporter gene, as well as functional knockout of endogenous human genes *CXCR4* and *TP53*. Although acting in a hit-and-run fashion, knockout efficiencies of our transient particles corresponded to 52%–80% of those obtained from constitutively active integrating vectors. Stable SpCas9 overexpression at high doses in murine NIH3T3 cells caused a substantial G0/G1 arrest accompanied by reduced cell growth and metabolic activity, which was prevented by transient *SpCas9* transfer. In summary, the non-integrating retrovirus-based vector particles introduced here allow efficient and dose-controlled delivery of CRISPR/Cas9 components into target cells.

INTRODUCTION

The development of the novel RNA-guided endonuclease (RGEN) genome editing technology CRISPR/Cas9 has revolutionized the world of life sciences. The CRISPR/Cas9 nuclease system is derived from archaea and bacteria and represents an adaptive immune mechanism that protects prokaryotes from invading phages or plasmids.[1,2] In its native form, CRISPR/Cas9 acts as a three component ribonucleoprotein (RNP) complex that consists of the Cas9 enzyme, the mature *trans*-activating CRISPR RNA (tracrRNA), and the CRISPR RNA (crRNA).[3,4] The latter encodes the 20-nucleotide-long protospacer, which is complementary to the target DNA sequence and responsible for precise guidance of Cas9 to the locus. However, ultimate target DNA cleavage is only initiated if a protospacer adjacent motif (PAM) is located next to the target sequence. CRISPR/Cas9 has become a prominent tool in the field of genetic engineering, with the most commonly used representative derived from *Streptococcus pyogenes* (*Sp*).[5] To enable CRISPR/Cas9-based genome editing in eukaryotic cells, the *SpCas9* coding sequence was codon optimized for efficient codon usage in respective target cells, and nuclear targeting of the enzyme was ensured by the introduction of two nuclear localization signals (NLSs).[6–9] Genetic fusion of tracrRNA and crRNA to one single-guide RNA (sgRNA) further simplified the technique.[10] Expression of both components in eukaryotic cells induces double-strand breaks (DSBs) at the respective target sequence, which can then undergo DNA repair by non-homologous end joining (NHEJ) or homology-directed repair (HDR) mechanisms.[11] While NHEJ-mediated DNA repair is prone to errors and introduces insertions or deletions (InDels) at the cleavage site, HDR is capable of precisely repairing the disrupted locus when a template DNA molecule is available. Precise and efficient induction of DSBs at selected DNA loci and the associated stimulation of the endogenous cellular repair machinery combine to make CRISPR/Cas9 a promising technology for human gene and cell therapies. Gene therapy trials with designer nucleases, such as zinc finger or transcription activator-like effector nucleases, have already entered the clinical arena, and clinical evaluation of novel approaches using CRISPR/Cas9 have just begun or will follow in the

Received 6 April 2018; accepted 7 September 2018;
https://doi.org/10.1016/j.omtn.2018.09.006.

Correspondence: Axel Schambach, MD, PhD, Institute of Experimental Hematology, Hannover Medical School, Carl-Neuberg-Strasse 1, Hannover 30625, Germany.
E-mail: schambach.axel@mh-hannover.de
Correspondence: Melanie Galla, PhD, Institute of Experimental Hematology, Hannover Medical School, Carl-Neuberg-Strasse 1, Hannover 30625, Germany.
E-mail: galla.melanie@mh-hannover.de

near future.[12,13] Therefore, efficient and safe delivery of CRISPR/Cas9 components to target cells is a prerequisite for successful gene editing therapies. Because cytotoxic side effects and/or off-target events were described for overexpression of several nucleases, such as *Cre* recombinase,[14–16] *Sleeping Beauty transposase*,[17] or zinc finger nucleases (ZFNs),[18–20] the CRISPR/Cas9 complex should ideally be transiently expressed to avoid stable and long-term expression of this DNA-modifying enzyme. Multiple studies have shown that transient expression of DNA-modifying enzymes minimizes cytotoxicity and/or off-target events.[16,17,21–24] The most widely used transient methods to introduce the CRISPR/Cas9 components into target cells are transfection (e.g., electroporation) of *SpCas9* and sgRNA-encoding plasmids and delivery of SpCas9 as purified protein or as *in vitro* transcribed mRNA, together with the sgRNA. These protocols were shown to be less cytotoxic and highly successful in achieving high levels of gene editing, even in primary cells.[21,25–27] Nevertheless, viral vectors that are derived from wild-type viruses, which have optimized cell entry during evolution, are still the vehicle of choice for many applications. Exploiting the evolved viral properties maximizes the efficiency and minimizes the cytotoxicity of delivery.[28] So far, various non-integrating viral vectors have been used to deliver gene editing tools to target cells. Among these, adeno-associated viral (AAV) or adenoviral (Adv) vector systems were shown to efficiently deliver CRISPR/Cas9 components into various cell types.[29,30] However, Adv vectors display high immunogenicity *in vivo*, and the better-tolerated AAV vectors exhibit a limited packaging capacity of ~4.8 kilobases (kb) of DNA.[31,32] This has the consequence that *SpCas9* with a coding sequence of ~4 kb and the sgRNA expression cassettes require co-delivery via two separate AAV vector particles. Integrase-deficient retroviral vectors represent additional transient and low-immunogenic viral vector tools successfully used for CRISPR/Cas9 delivery.[33] Retroviral vectors follow the early life cycle of wild-type retroviruses and are mostly derived from lentiviral HIV-1 or the gammaretroviral murine leukemia virus (MLV), which are abbreviated here as lentiviral integrating transfer (LIT) or retroviral integrating transfer (RIT). Targeted interference with different steps of the retroviral life cycle allows conversion of stably integrating vectors into transient retroviral vector tools.[34–36] Integrase-deficient retroviral vectors harbor point mutations within the catalytic domain of the viral integrase (IN), resulting in the establishment of extra-chromosomal episomal DNA, which is gradually diluted upon cell division. However, the presence of episomal DNA could still provoke residual integration events, especially when DNA-modifying enzymes that can induce DSBs are delivered.[37] An alternative and safer strategy would be the transfer of DNA-modifying enzymes as RNA or even protein by retroviral particles,[16,38–40] which allows dose-controlled delivery in a hit-and-run fashion. We previously showed successful transient and non-cytotoxic delivery of *Sleeping Beauty transposase* and *Cre* and *Flp* recombinases via retrovirus-mediated mRNA transfer (RMT) particles, which are deficient in reverse transcription.[17,41] Moreover, fusion of Flp recombinase to retroviral structural Gag proteins (e.g., matrix [MA] and nucleocapsid [NC]) allowed efficient excision of FLP recognition target (FRT)-flanked reprogramming cassettes in murine and human induced pluripotent stem cells.[36,42] Retroviral delivery of RNA and/or proteins does not involve a DNA intermediate and thus excludes the possibility of residual DNA integration events. Another possibility for RNA delivery is to exploit the MS2 bacteriophage packaging machinery within retroviral vector particles. The packaging system of the MS2 bacteriophage is composed of two major components, the MS2 coat protein and a short RNA hairpin-stem loop structure of ~23 nucleotides. The MS2 coat protein dimer binds to the stem loop sequence on the RNA, which enables encapsidation of the bacteriophage RNA in the MS2 particle.[43–45] This targeted interaction is used for various applications, including protein tethering to nucleic acids and mRNA imaging.[46] In a more recent study, the MS2 system was used to create lentivirus-MS2 virus-like particle chimera to transfer non-viral RNAs for the delivery of luciferase, *Cre* recombinase, and transcription factors *in vitro* and *in vivo*.[47]

In the present study, we developed non-integrating MLV-based CRISPR/Cas9 all-in-one particles for targeted gene knockout. We achieved efficient co-delivery of non-viral *SpCas9* mRNA and sgRNA transcripts into target cells by replacement of retroviral components with analogous parts of the MS2 phage packaging machinery. Proof of concept was obtained by efficient knockout of a surrogate CRISPR/Cas9 reporter gene in human and murine cell lines. Furthermore, we disrupted endogenous genes and showed functional knockout of the chemokine receptor *CXCR4* in a human T cell line and a *TP53* knockout-driven proliferative advantage of primary newborn human foreskin fibroblasts (NUFFs) under competitive culture conditions. In addition, we demonstrated a previously unknown dose-dependent cytotoxicity of SpCas9 expression, which occurred even in the absence of a co-expressed sgRNA. High-dose and prolonged SpCas9 expression triggered a substantial G0/G1 cell-cycle arrest and was associated with reduced cell growth and metabolic activity. Short-term expression of SpCas9 via our transient particles abolished these effects. In conclusion, our Gag.MS2.CRISPR/Cas9 all-in-one particles represent a versatile tool for efficient, dose-controlled, and non-toxic delivery of CRISPR/Cas9 RNAs into target cells.

RESULTS

Design of Gag.MS2 and Non-Retroviral SpCas9 and sgRNA Expression Plasmids

Based on the concept of non-integrating RMT, we aimed to develop MLV-based particles as vehicles for the transfer of CRISPR/Cas9 RNAs into target cells. Wild-type retroviruses and their integrating and non-integrating vector derivatives usually contain two copies of their plus-stranded, capped, and polyadenylated mRNA genome,[48] which are packaged in a highly specific manner through binding of the NC domain of the retroviral Gag polyprotein to the retroviral packaging signal Ψ located on the viral genome. We exploited this property during development of RMT to deliver mRNA.[16] However, targeted gene knockout via CRISPR/Cas9 requires *Cas9* mRNA transfer and co-delivery of an RNA polymerase (Pol) III-driven sgRNA transcript. To allow for specific co-packing of

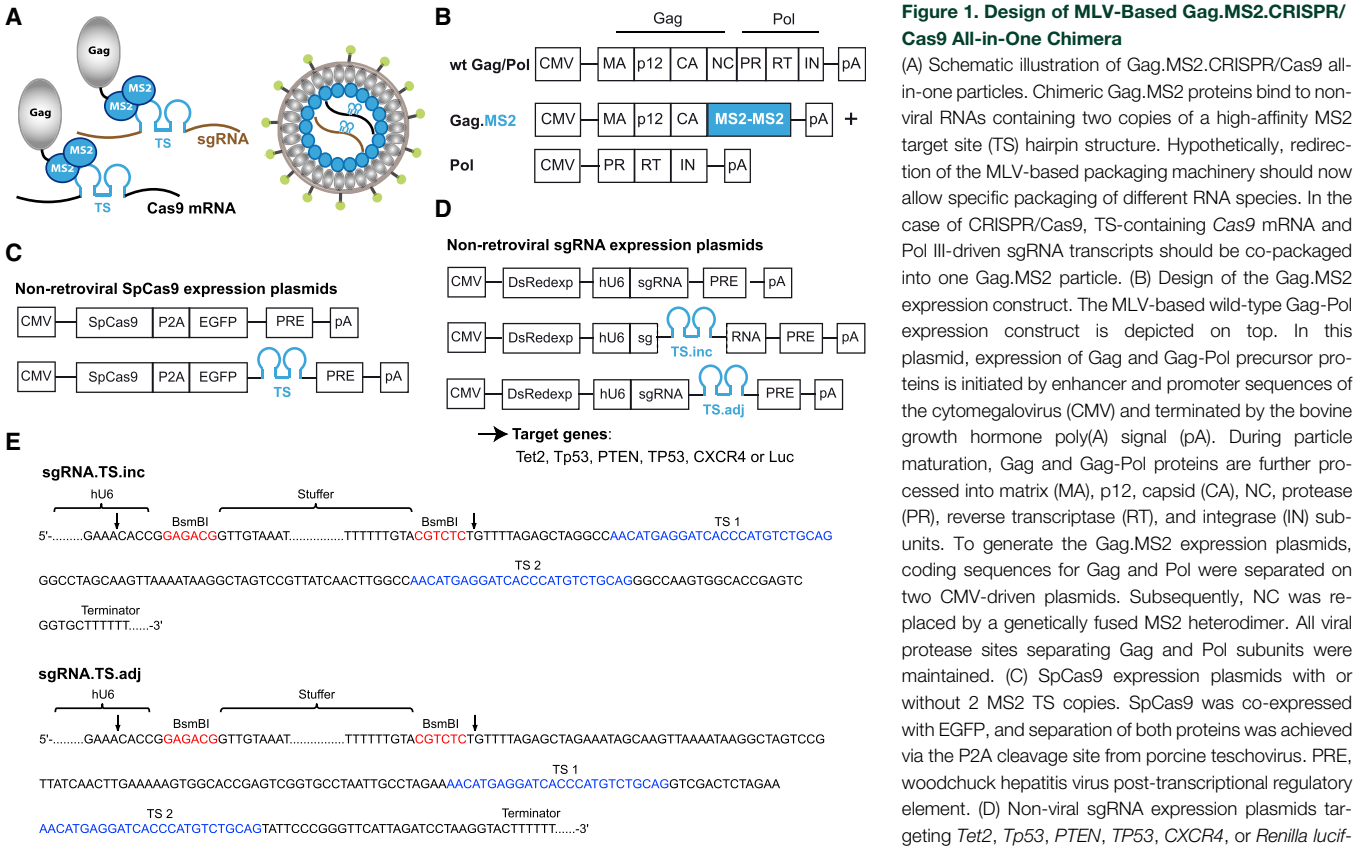

Figure 1. Design of MLV-Based Gag.MS2.CRISPR/Cas9 All-in-One Chimera

(A) Schematic illustration of Gag.MS2.CRISPR/Cas9 all-in-one particles. Chimeric Gag.MS2 proteins bind to non-viral RNAs containing two copies of a high-affinity MS2 target site (TS) hairpin structure. Hypothetically, redirection of the MLV-based packaging machinery should now allow specific packaging of different RNA species. In the case of CRISPR/Cas9, TS-containing *Cas9* mRNA and Pol III-driven sgRNA transcripts should be co-packaged into one Gag.MS2 particle. (B) Design of the Gag.MS2 expression construct. The MLV-based wild-type Gag-Pol expression construct is depicted on top. In this plasmid, expression of Gag and Gag-Pol precursor proteins is initiated by enhancer and promoter sequences of the cytomegalovirus (CMV) and terminated by the bovine growth hormone poly(A) signal (pA). During particle maturation, Gag and Gag-Pol proteins are further processed into matrix (MA), p12, capsid (CA), NC, protease (PR), reverse transcriptase (RT), and integrase (IN) subunits. To generate the Gag.MS2 expression plasmids, coding sequences for Gag and Pol were separated on two CMV-driven plasmids. Subsequently, NC was replaced by a genetically fused MS2 heterodimer. All viral protease sites separating Gag and Pol subunits were maintained. (C) SpCas9 expression plasmids with or without 2 MS2 TS copies. SpCas9 was co-expressed with EGFP, and separation of both proteins was achieved via the P2A cleavage site from porcine teschovirus. PRE, woodchuck hepatitis virus post-transcriptional regulatory element. (D) Non-viral sgRNA expression plasmids targeting *Tet2*, *Tp53*, *PTEN*, *TP53*, *CXCR4*, or *Renilla luciferase* (Luc). sgRNAs with or without TS hairpins were generated. Two TS hairpins were either incorporated (TS.inc) into or cloned adjacent (TS.adj) to the sgRNA scaffold. To control for transfection efficiencies, a CMV-driven red-fluorescent *DsRedexp* expression cassette was included. hU6, human RNA polymerase III U6 promoter. (E) Detailed overview of TS.inc and TS.adj expression cassettes. The scaffold sequence of TS.inc is depicted on top, and the scaffold sequence of TS.adj is at the bottom. Both sgRNAs contain a 105 bp long stuffer sequence flanked by BsmBI restriction sites (red). The design of the TS.inc scaffold was adapted from Konermann et al.,[54] and positioning of the two TS hairpins in the TS.adj constructs was based on the work of Mali et al.[55] with differences in TS linker and spacer sequences. The positions of the two TS hairpins (TS 1 and TS 2) are marked in blue. The arrows point to the cutting sites of BsmBI. Expression of the sgRNAs is terminated by the TTTTTT motif.

Pol II- and Pol III-derived RNAs into one particle, we redirected the retroviral packaging system and designed chimeric MLV-based MS2 particles (Figure 1A). Replacement of Ψ by the MS2 target site (TS) RNA hairpin structure and incorporation of the MS2 coat protein into the retroviral Gag precursor should enable packaging of various RNA species. Thus, we separated the gammaretroviral Gag from the Pol open reading frame and replaced NC within Gag by a genetically fused MS2 protein heterodimer[49] downstream of the viral protease site that separates the retroviral capsid (CA) from the NC protein (Figure 1B). As a refinement, we constructed plasmids to express TS-containing *SpCas9* mRNA or respective Pol III-driven sgRNA transcripts devoid of any retroviral sequences (Figures 1C and 1D). Identically constructed plasmids lacking TS were also generated. SpCas9 was co-expressed with EGFP via the P2A cleavage site from porcine teschovirus (Figure 1C). To enhance *SpCas9.P2A.EGFP* mRNA nuclear export and stability, and therefore expression and packaging, we incorporated the full-length 900-bp fragment of the woodchuck hepatitis virus post-transcriptional regulatory element (PRE).[50–52] The TS-carrying SpCas9 (SpCas9.TS) plasmid was generated by inserting two copies of a high-affinity TS hairpin mutant[53] between *EGFP* and PRE. To express TS-containing sgRNAs, we designed red fluorescent *DsRedexp*-encoding plasmids that co-express the respective sgRNAs under control of the human Pol III U6 (hU6) promoter (Figure 1D). Similar to recent studies, we designed two TS-containing sgRNA backbones and incorporated two TS high-affinity hairpins either within (TS.inc) or adjacent (TS.adj) to the sgRNA scaffold.[54,55] To facilitate cloning of targeting protospacer sequences into the sgRNA.TS backbones, we inserted a non-coding stuffer sequence flanked by BsmBI restriction sites upstream of the sgRNA scaffold (Figure 1E), which allows easy and fast replacement of the stuffer by desired targeting guide sequences that can be introduced as annealed and phosphorylated oligonucleotides (see also Supplemental Materials and Methods).

Generation of CRISPR/Cas9 Surrogate Reporter Cells and Validation of TS-Encoding Expression Plasmids

To test our Gag.MS2 particles, we generated human and mouse CRISPR/Cas9 reporter cell lines (Figure S1) and initial experiments

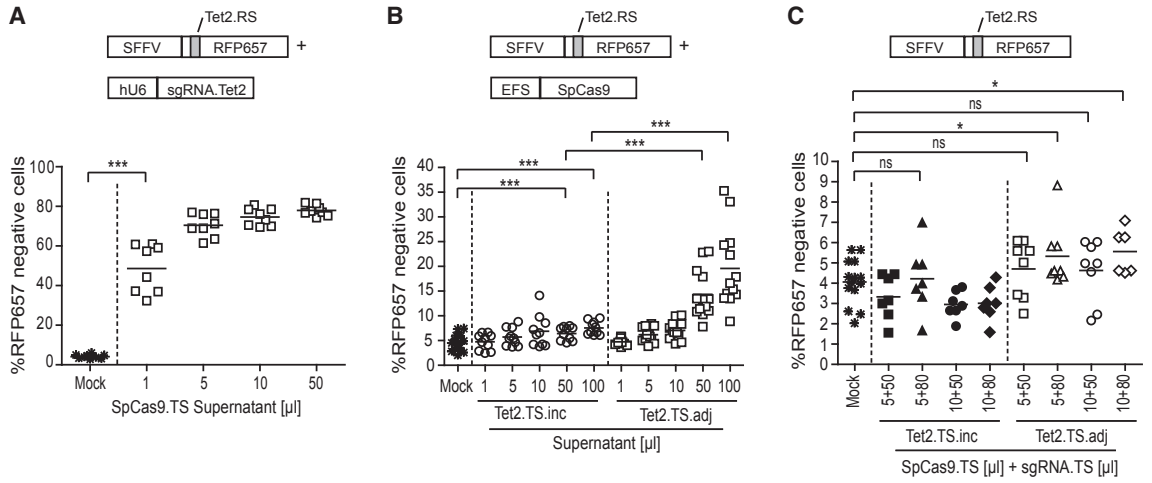

Figure 2. Individual Transfer of CRISPR/Cas9 RNAs by Gag.MS2 Particles

(A) Highly efficient delivery of *SpCas9.TS* mRNA into target cells. Gag.MS2.SpCas9.TS particles were used to transduce NIH3T3-based RFP657.Tet2+sgRNA.Tet2 reporter cells (see the scheme above the graph) with the depicted supernatant volumes. The percentage of RFP657-negative cells was determined 6 days post-transduction. The results of 8 independent supernatants are shown. (B) Inefficient transfer of sgRNAs Tet2.TS.inc and Tet2.TS.adj by Gag.MS2 particles. RFP657.Tet2+SpCas9 NIH3T3 reporter cells were transduced with Tet2.TS.inc or Tet2.TS.adj Gag.MS2 particles. *RFP657* knockout was determined by flow cytometry 6 days post-transduction. The results of 10 (Tet2.TS.inc) to 13 (Tet2.TS.adj) independently packaged supernatants are shown. (C) Co-transduction of separately packaged *SpCas9.TS* mRNA and sgRNA.TS resulted in poor *RFP657* knockout rates. NIH3T3-based RFP657.Tet2 reporter cells were transduced with 6–8 individually packaged SpCas9.TS and Tet2.TS.inc or Tet2.TS.adj Gag.MS2 supernatants from (A) and (B) at the depicted volume ratios. Flow cytometry was performed 6 days post-transduction.

were accomplished with the recently published and validated sgRNA.Tet2, which targets the mouse *Tet methylcytosine dioxygenase 2* (*Tet2*) gene (Table S1).[56] In these reporter cells, successful CRISPR/Cas9-mediated, site-specific cleavage is indicated by the loss of RFP657 expression, because the *RFP657* cDNA contains the respective Tet2 recognition site (RS) sequence downstream of its ATG start codon (Figure S1A). We generated three types of Tet2-based CRISPR/Cas9 reporter cells: (1) cells that only contain the *RFP657.Tet2* reporter cassette (RFP657.Tet2 reporter), (2) cells that co-express the RFP657.Tet2 reporter and SpCas9 (RFP657.Tet2+SpCas9 reporter), and (3) cells that express RFP657.Tet2 with sgRNA.Tet2 (RFP657.Tet2+sgRNA.Tet2 reporter). All reporter cells were validated by stable retroviral delivery of the respective CRISPR/Cas9 components before further use (Figures S1B–S1F). Next, we evaluated the influence of the TS hairpins on SpCas9 and sgRNA expression and/or performance. Thus, we transfected the respective mouse or human Tet2-based CRISPR/Cas9 reporter cells with wild-type (no TS) or TS-encoding plasmids (Figure S2) and determined the transfection and *RFP657* knockout efficiencies 2 and 10 days after transfection, respectively. When only SpCas9 (Figure S2A) or sgRNA.Tet2 (Figure S2B) expression plasmids were delivered, relative *RFP657* knockout rates revealed no significant TS-related restriction compared to wild-type constructs. However, placement of the TS dimer adjacent to the sgRNA scaffold seemed to enhance activity. Furthermore, mean knockout rates in co-transfected RFP657.Tet2 reporter cells (Figure S2C) tended to be higher in samples that were transfected with wild-type SpCas9 and sgRNA.Tet2 expression plasmids. Nevertheless, up to 50% knockout of *RFP657* was achieved in cells that were co-transfected with TS-containing SpCas9 and sgRNA.Tet2 expression plasmids. Therefore, we proceeded with these constructs.

Transient Individual Delivery of CRISPR/Cas9 Components into RFP657.Tet2 Reporter Cells by Gag.MS2 Particles

To test whether TS-containing CRISPR/Cas9 RNAs are efficiently packaged by Gag.MS2 molecules, we individually packaged *SpCas9.*TS mRNA, Tet2.TS.inc sgRNA, or Tet2.TS.adj sgRNA into Gag.MS2 particles pseudotyped with the envelope glycoprotein from the vesicular stomatitis virus (VSVg). To allow the MS2 dimer protein to be cleaved from CA by the viral protease during Gag maturation, we also included an MLV-based Pol expression plasmid during particle generation (Figure 1B). Subsequently, we concentrated the formed particles 50-fold and transduced respective murine (Figure 2) or human (Figure S3) RFP657.Tet2 reporter cells with increasing amounts of the corresponding supernatant. Delivery of *SpCas9.TS* mRNA into RFP657.Tet2+sgRNA.Tet2 reporter cells (Figure 2A and Figure S3A) was far more efficient than the transfer of Pol III-derived short, uncapped, and non-polyadenylated Tet2.TS transcripts into RFP657.Tet2+SpCas9 reporter cells (Figures 2B and S3B). While application of Gag.MS2.SpCas9.TS particles yielded up to 82% knockout of *RFP657* in human and murine RFP657.Tet2+sgRNA.Tet2 reporter cells, *RFP657* knockout rates by Tet2.TS sgRNA variants were clearly reduced and exhibited better activity in murine RFP657.Tet2+SpCas9 than in human reporter cells (compare Figures 2B and S3B). As apparent in Figure S2B, Gag.MS2.Tet2.TS.adj particles performed significantly better than the Tet2.TS.inc counterparts and resulted in knockout rates of up to 32% in murine RFP657.Tet2+SpCas9 reporter cells. A higher

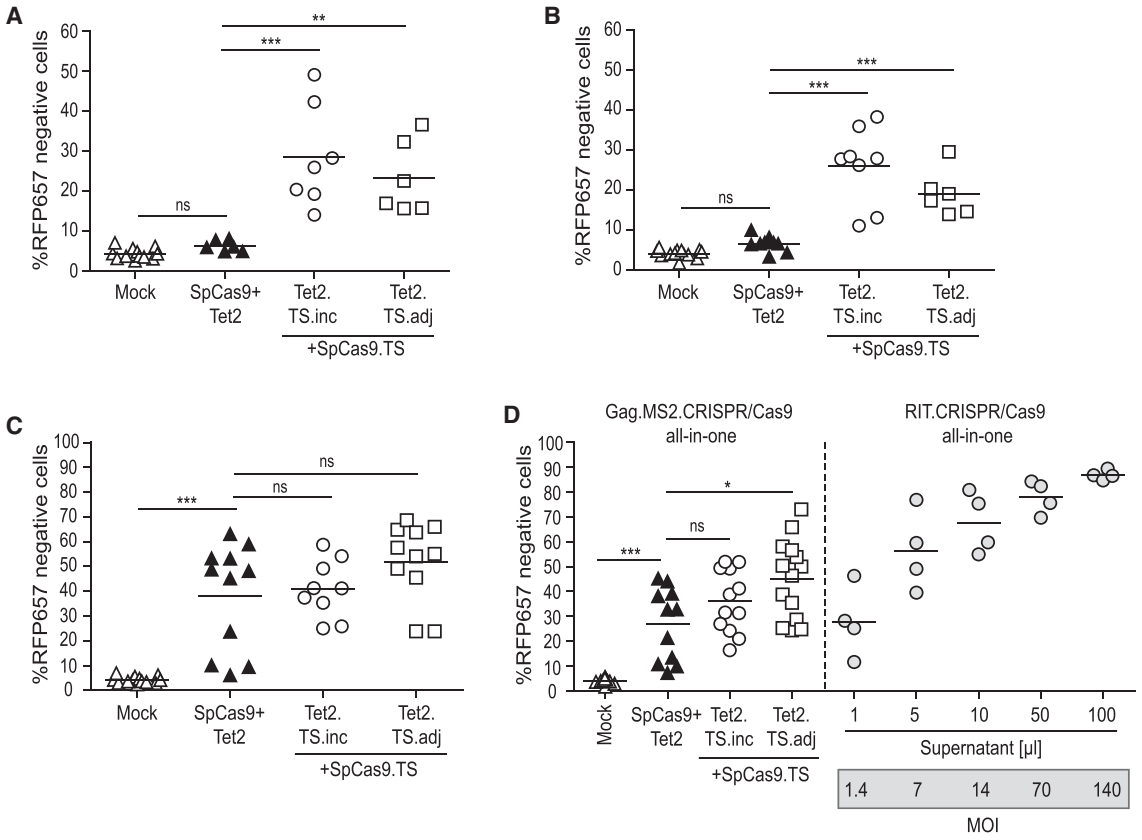

Figure 3. Efficient *RFP657* Knockout by Gag.MS2.CRISPR/Cas9 All-in-One Particles

SpCas9, Tet2 sgRNA, Gag.MS2, Pol, and VSVg expression plasmids were co-transfected into the HEK293T packaging cell line. The resulting supernatants SpCas9+Tet2, SpCas9.TS+Tet2.TS.inc, or SpCas9.TS+Tet2.TS.adj were harvested and concentrated 50-fold. Transfection efficiencies were determined for all produced supernatants (see also Figures S4A and S4B). (A and B) Efficient delivery of CRISPR/Cas9 RNA components depends on the presence of the TS hairpin dimer. Supernatants from HEK293T cells that exhibited transfection efficiencies <50% were used to transduce NIH3T3-based (A) or HT1080-based (B) RFP657.Tet2 reporter cells. The graphs show *RFP657* knockout rates mediated by 100 µL supernatant for the individual experiments 5–6 days post-transduction. Results from 4–7 independently generated supernatants are displayed (SpCas9+Tet2 = 6 supernatants, SpCas9.TS+Tet2.TS.inc = 7 supernatants, and SpCas9.TS+Tet2.TS.adj = 4 supernatants) (see also Figure S4A). (C and D) Non-specific packaging of CRISPR/Cas9 RNAs and/or RNPs into Gag.MS2 particles. Experiments were similar to those shown in (A) and (B). However, NIH3T3 (C) and HT1080 (D) RFP657.Tet2 reporter cells were transduced with supernatants that were obtained from transfections with efficiencies >50%. The depicted results were generated with 100 µL of 10–12 individually packaged supernatants (SpCas9+Tet2 = 10 supernatants, SpCas9.TS+Tet2.TS.inc = 10 supernatants, and SpCas9.TS+Tet2.TS.adj = 12 supernatants) (see also Figure S4B). The graph depicted in (D) also displays *RFP657* knockout rates induced by different volumes of 50-fold-concentrated integrating RIT.CRISPR/Cas9.Tet2 all-in-one supernatants. The respective MOIs are given in the gray box. Each data point represents an individually generated supernatant (n = 4) with an average functional titer of 7.2×10^7 t.u./mL.

concentration (170-fold) of Tet2.TS sgRNA Gag.MS2 supernatants slightly increased knockout rates in human RFP657.Tet2+SpCas9 reporter cells (Figure S3B, left versus right graph) but remained far below knockout rates obtained in murine RFP657.Tet2+SpCas9 reporter cells by treatment with Gag.MS2.Tet2.TS.adj particles. Thereafter, we co-transduced human and mouse RFP657.Tet2 reporter cells with separately generated SpCas9.TS and Tet2.TS Gag.MS2 particles (Figures 2C and S3C). Because sufficient Gag.MS2-mediated sgRNA delivery turned out to be limiting, we provided the Tet2.TS.inc or Tet2.TS.adj sgRNA supernatants in excess. However, murine and human RFP657.Tet2 reporter cells revealed mostly marginal and inconsistent *RFP657* knockout rates. Only co-transduction of SpCas9.TS and 16-fold more Tet2.TS.adj supernatant showed low but significant *RFP657* knockout in both reporter cells.

Efficient Targeted *RFP657* Knockout by Gag.MS2.CRISPR/Cas9 All-in-One Particles

Because co-transduction of individually packaged CRISPR/Cas9 components was clearly suboptimal, we hypothesized that co-packaging of *SpCas9.TS* and Tet2.TS.inc or Tet2.TS.adj RNAs into the same particle would increase *RFP657* knockout rates. Therefore, we packaged *SpCas9.TS* and Tet2.TS.inc or Tet2.TS.adj into VSVg-pseudotyped Gag.MS2 particles and transduced murine and human RFP657.Tet2 reporter cells (Figures 3 and S4). Supernatants generated with wild-type SpCas9 and sgRNA.Tet2 expression plasmids,

which lack the TS hairpin dimer, were included as controls. Transduction of mouse and human RFP657.Tet2 reporter cells with 50-fold concentrated SpCas9.TS+Tet2.TS.inc or SpCas9.TS+Tet2.TS.adj Gag.MS2 all-in-one particles resulted in efficient *RFP657* knockout of up to ~70%. The efficacy of Gag.MS2.CRISPR/Cas9 all-in-one particles depended on the transfection efficiency during particle generation. Supernatants derived from HEK293T packaging cells that exhibited transfection rates <50% were less efficient (Figures 3A, 3B, and S4A) than supernatants harvested from cells that were transfected >50% (Figures 3C, 3D, and S4B–S4D). As expected, SpCas9+Tet2 supernatants (no TS) derived from transfections of <50% showed no significant *RFP657* knockout when compared to non-treated Mock samples (Figures 3A and 3B). However, transduction with SpCas9+ sgRNA.Tet2 Gag.MS2 supernatants (no TS) from transfections of >50% resulted in slightly lower (compared to SpCas9.TS+Tet2.TS.inc or SpCas9.TS+ Tet2.TS.adj) but significant *RFP657* knockout in murine and human reporter cells (Figures 3C, 3D, S4C, and S4D), indicating that Gag.MS2 may accomplish non-specific packaging of CRISPR/Cas9 RNA and/or SpCas9/sgRNA RNP complexes that do not contain the TS. Side-by-side comparison of Gag.MS2 with commonly used integrating RIT.CRISPR/Cas9 all-in-one supernatants revealed comparable *RFP657* knockout rates (depending on the MOI of the integrating vector) in human RFP657.Tet2 reporter cells (Figure 3D). 100 μL Gag.MS2.CRISPR/Cas9.Tet2.TS.adj supernatant (transfection efficiency >50%) resulted in an average *RFP657* knockout of ~45%, which corresponds to 52% (100 μL, MOI 140) to 80% (5 μL, MOI 7) of the average knockout levels achieved with the RIT.CRISPR/Cas9.Tet2 all-in-one supernatants.

To explore whether suspension cells are also susceptible to our particles, we generated RFP657.Tet2 suspension reporter cells based on human Jurkat T lymphocytes and transduced them with SpCas9.TS+ Tet2.TS.inc or SpCas9.TS+Tet2.TS.adj Gag.MS2 particles (Figure S5). Both particle types showed efficient *RFP657* knockout in Jurkat-based RFP657.Tet2 reporter cells. Treatment of cells with SpCas9.TS+ Tet2.TS.adj particles resulted in significantly higher *RFP657* knockout rates when compared to SpCas9.TS+Tet2.TS.inc particles.

Characterization of Gag.MS2 Particles

The observed *RFP657* knockout rates achieved by SpCas9+Tet2 Gag.MS2 control particles (Figures 3C, 3D, S4C, and S4D) suggest that not only TS-containing CRISPR/Cas9 RNA but also, to a lesser extent, SpCas9/sgRNA RNP complexes are transferred into cells by our chimeric Gag.MS2.CRISPR/Cas9 all-in-one particles. Thus, we determined the abundance of CRISPR/Cas9 RNA transcripts and/or SpCas9 protein in our Gag.MS2 particles, which were produced from HEK293T cells with a transfection efficiency >50%. We generated 100-fold concentrated Gag.MS2 particles in the presence of TS- or no TS-encoding SpCas9 and/or Tet2 expression plasmids. The supernatants were subjected to extensive DNase treatment and analyzed for *SpCas9* mRNA and/or Tet2 sgRNA content (Figure 4; Table 1). First, we analyzed individually packaged SpCas9 and Tet2 Gag.MS2 particles and found Tet2 sgRNA and *SpCas9* mRNA transcripts within the supernatants irrespective of the TS (Figures 4A and 4B). However, the presence of TS clearly improved packaging of the transcripts and resulted in a 12-fold higher *SpCas9* mRNA level or 71-fold (TS.adj) to 142-fold (TS.inc) higher sgRNA.Tet2 levels within Gag.MS2 particles. Furthermore, the different Tet2 sgRNAs are more abundant in Gag.MS2 particles than the *SpCas9* mRNA, arguing for better packaging of small RNAs. This phenomenon was also observed in Gag.MS2.CRISPR/Cas9.Tet2 all-in-one particles, where the Tet2.TS sgRNA content was determined to be 74-fold (SpCas9.TS+ Tet2.TS.inc) to 152-fold (SpCas9.TS+Tet2.TS.adj) higher than the *SpCas9.TS* mRNA content (Table 1). In contrast to individual sgRNA.Tet2 Gag.MS2 particles, Gag.MS2.CRISPR/Cas9 all-in-one particles showed ~2-fold more packaging of Tet2.TS.adj than of Tet2.TS.inc. Next, we analyzed individually packaged SpCas9 Gag.MS2 particles and Gag.MS2.CRISPR/Cas9.Tet2 all-in-one particle preparations by immunoblot and detected SpCas9 protein in all settings (Figure 4C). To more closely quantify SpCas9 protein levels, we performed an SpCas9 ELISA and determined similar amounts of SpCas9 protein in all analyzed supernatants, with an average concentration of 24 ng/50 μL (Figure 4D; Table 1). Finally, we analyzed the occurrence of stable integration events and determined the mean vector copy number (VCN) via real-time PCR in cultures 10 days post-transduction with Gag.MS2.CRISPR/Cas9.Tet2 all-in-one vectors (Figure 4E). Stably integrating RIT.CRISPR/Cas9.Tet2 all-in-one vector particles served as positive controls. *SpCas9*, and the DNA sequence encoding for the Tet2 sgRNA was only detected in the genomic DNA (gDNA) of cultures that were transduced with integrating RIT.CRISPR/Cas9.Tet2 all-in-one particles, demonstrating that transfer of *SpCas9.TS* and/or Tet2.TS.adj/Tet2.TS.inc RNA via Gag.MS2 particles was transient. In summary, Gag.MS2 efficiently packaged TS-containing RNAs and transiently transferred these RNAs into target cells, but the respective particles may also contain remnants of non-specifically packaged RNAs and/or SpCas9 proteins.

Cell-Cycle Arrest Mediated by Constitutive High-Dose SpCas9 Expression

We and others have demonstrated that overexpression of DNA-modifying enzymes alone was sufficient to cause cytotoxicity.[14–19,57] Therefore, we examined NIH3T3 cells that stably expressed SpCas9 in the absence of a respective sgRNA for signs of toxicity and cell death (Figure 5). We compared integrating RIT.SpCas9 with integrating RIT.EGFP or transient Gag.MS2.SpCas9.TS vector particles. After particle generation, all supernatants were initially tested for their functionality in the respective cell lines (Figure S6). We determined the functional titers of RIT.EGFP and RIT.SpCas9 supernatants (Figure S6A) and tested *SpCas9*-encoding RIT.SpCas9 and Gag.MS2.SpCas9.TS particles for their *RFP657* knockout efficiency (Figures S6B and S6C). All supernatants were functional in terms of transgene expression, and RIT.EGFP and RIT.SpCas9 supernatants revealed functional titers on average of 5.17×10^9 transducing units (t.u.)/mL and 1.24×10^9 t.u./mL, respectively. Because we aimed to apply equal particle amounts per cell for our cytotoxicity assays, we also titrated integrating and non-integrating supernatants via real-time qRT-PCR (Figure S6D). To capture only particles that are

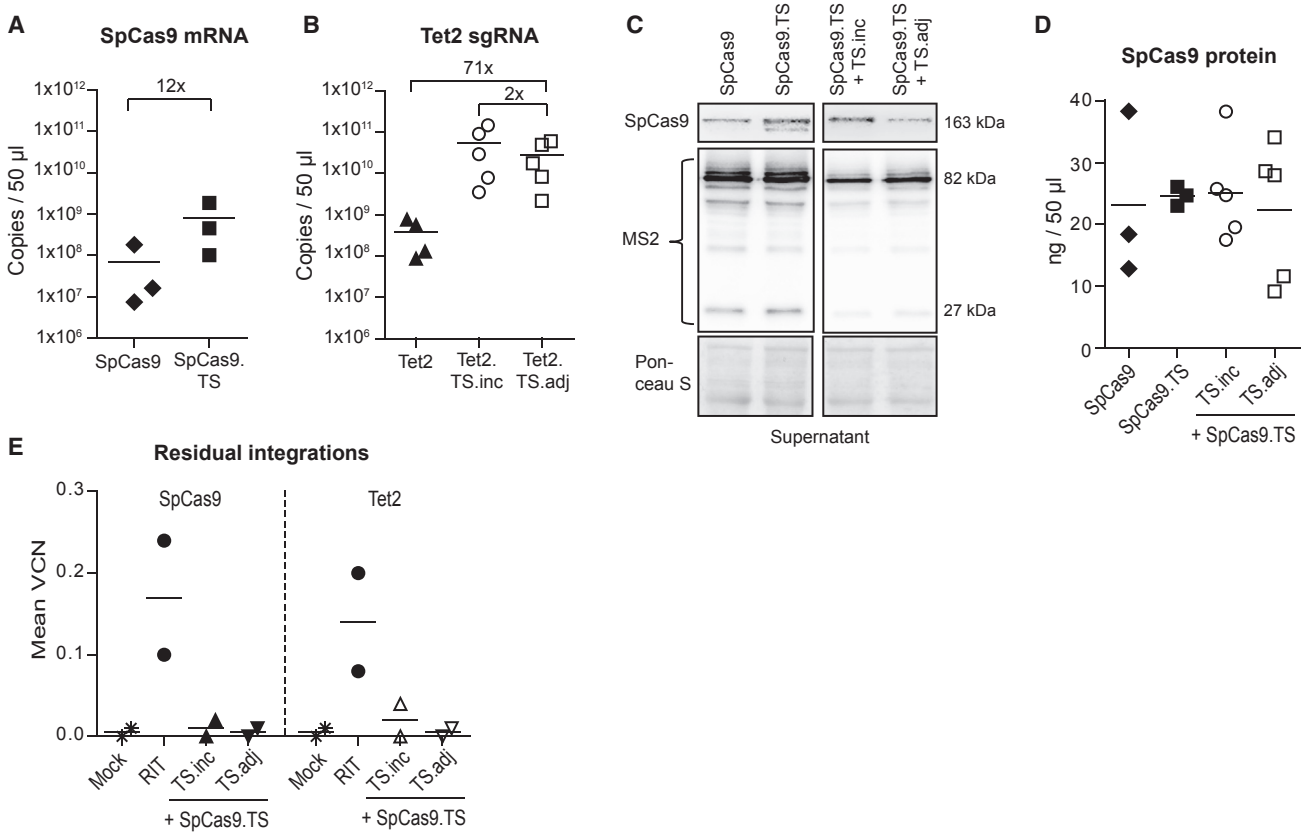

Figure 4. Characterization of Gag.MS2.CRISPR/Cas9 Particles

(A) *SpCas9* and *SpCas9.TS* mRNA content of individually packaged Gag.MS2 particles. Absolute mRNA copies per 50 µL supernatant are shown. (B) Tet2 sgRNA quantification. The differences of incorporated Tet2 (no TS), Tet2.TS.inc, or Tet2.TS.adj sgRNAs are shown. The graph depicts the sgRNA copies per 50 µL. Absolute amounts were calculated with the help of individual standards. (C) Gag.MS2.CRISPR/Cas9 supernatants contain SpCas9 protein. SpCas9, SpCas9.TS, SpCas9.TS+Tet2.TS.inc (TS.inc), and SpCas9.TS+Tet2.TS.adj (TS.adj) Gag.MS2 supernatants were subjected to immunoblot analysis, and membranes were successively stained with Ponceau S for total, SpCas9 (163 kDa), and MS2 dimer (27 kDa) proteins. The 82 kDa band on the MS2 blot represents the immature Gag.MS2 precursor polyprotein. (D) Quantification of SpCas9 protein by ELISA within different particle types. Each data point represents one independent supernatant. (E) Chimeric Gag.MS2.CRISPR/Cas9 all-in-one particles do not integrate. The genomic DNA of transduced cells was harvested 10 days post-transduction and analyzed for the occurrence of stable integration events. The graph depicts the determined mean vector copy numbers (VCNs) of two independently generated supernatants. An integrating RIT.CRISPR/Cas9.Tet2 all-in-one vector served as a positive control (average transduction rate: 14% EGFP-positive cells). Each data point represents the mean value of 3 independently determined C_t values (technical replicates).

functional in cellular entry, we determined the relative amount of incoming mRNA vector genomes for each supernatant 3 hr post-transduction. Comparable to the functional titers shown in Figure S6A, RIT.EGFP particles transferred ~4-fold more mRNA than RIT.SpCas9 particles. Although quite potent in *SpCas9* delivery as measured by *RFP657* knockout, Gag.MS2.SpCas9.TS particles delivered 46-fold less incoming *SpCas9* mRNA into cells than RIT.SpCas9 particles. To adjust RIT.EGFP and RIT.SpCas9 supernatants, we diluted RIT.EGFP supernatants with respective volumes of culture medium before transduction. Gag.MS2.SpCas9.TS supernatants were not adjusted to RIT.SpCas9 supernatants, because adjustment would have exceeded applicable volumes of supernatants. However, 50 µL Gag.MS2.SpCas9.TS is approximately equivalent (see the 46-fold factor calculated earlier) to 1 µL RIT.EGFP or RIT.SpCas9 supernatant. Based on the preceding determined functional titers (Figure S6A), 1 µL RIT.EGFP or RIT.SpCas9 corresponded to MOI ~13. We transduced wild-type NIH3T3 cells with the depicted supernatant volumes and determined the percentage of $EGFP^+$ cells 8 days post-transduction. As expected, integrating RIT.EGFP and RIT.SpCas9 revealed almost 100% $EGFP^+$ cultures, whereas EGFP expression was absent from cells that were transduced with non-integrating Gag.MS2.SpCas9.TS particles (Figure S6E). We next analyzed transduced and non-transduced Mock cultures for number of cells, metabolic activity, apoptosis, and cell-cycle abnormalities (Figure 5). In general, we observed within the first week after transduction reduced cell numbers (Figure 5A), and accordingly lower metabolic activity (Figure 5B) in cells that were transduced with RIT.EGFP or RIT.SpCas9 vectors compared to non-transduced Mock cultures. The negative effect of high-dose SpCas9 or EGFP expression was already visible at 1 µL and became more pronounced with increasing MOIs. However, cell proliferation and physiological activity was even more reduced in

Table 1. Detailed Analysis of Gag.MS2.CRISPR/Cas9 All-in-One Particles

Particle Type (CRISPR/Cas9.Tet2 All-in-One)	Tet2 sgRNA (Copies/50 μL)	*SpCas9* RNA (Copies/50 μL)	SpCas9 Protein (ng/50 μL)	%*RFP657* Knockout (50 μL)
RIT (no TS) n = 6 (functional titer: 6.7×10^7 t.u./mL)	ND	2.8×10^9–1.1×10^{10} ($4.9 \times 10^9 \pm 3.3 \times 10^9$)	ND	39.7–68.5 (57.8 ± 10.3)
Gag.MS2 (TS.inc) n = 5	1.0×10^9–1.8×10^{10} ($7.1 \times 10^9 \pm 7.1 \times 10^9$)	2.1×10^7–3.5×10^8 ($9.6 \times 10^7 \pm 1.4 \times 10^8$)	17.5–38.3 (25.2 ± 8.1)	21.2–54.9 (44.1 ± 13.2)
Gag.MS2 (TS.adj) n = 5	5.3×10^9–1.2×10^{11} ($5.8 \times 10^{10} \pm 4.5 \times 10^{10}$)	4.4×10^7–7.4×10^8 ($3.8 \times 10^8 \pm 3.2 \times 10^8$)	9.6–34.1 (22.3 ± 11.2)	33.3–81.4 (55.6 ± 22.9)

The abundance of Tet2 sgRNA, *SpCas9* mRNA, and SpCas9 protein was determined within 50 μL of 100-fold concentrated supernatants (n = 5). %*RFP657* knockout efficiency is depicted in the column on the right. For comparison, vector RNA genome (*SpCas9*) copies, mean functional titer, and *RFP657* knockout mediated by integrating RIT.CRISPR/Cas9.Tet2 all-in-one supernatants (n = 6) at average MOI 33.5 are shown. The amount of SpCas9 protein was measured with a SpCas9 ELISA. Ranges for individual supernatants are given, followed by the mean ± SD in parentheses. ND, not determined.

RIT.SpCas9-treated cultures, suggesting that stable ectopic SpCas9 expression is more cytotoxic than that of EGFP. In contrast, transduction of cells with 100 μL of non-integrating Gag.MS2.SpCas9.TS supernatant had no significant influence on cell growth or metabolic activity. To elucidate whether SpCas9-expressing cells die from apoptosis, we co-stained the cultures with Annexin V and propidium iodide (PI) 8 days post-transduction and observed elevated levels of Annexin V^+ cells (compared to RIT.EGFP) only in cultures that were treated with 50 μL of RIT.SpCas9 supernatant (MOI 650) (Figure 5C, left graph). A more detailed analysis of RIT.SpCas9-treated cultures revealed a dose-dependent increase of apoptotic (Annexin V^+) and dead (PI^+ or Annexin V^+/PI^+) cells, which again was most evident at the highest supernatant volume used (Figure 5C, right graph). Dissection of the cell cycle 6 days after particle application revealed a substantial G0/G1 arrest in cells transduced with RIT.SpCas9 (Figures 5D and S7). The G0/G1 arrest depended on the applied vector dose and started to manifest in cultures that were treated with 5 μL RIT.SpCas9 supernatant (MOI 65). No obvious cell-cycle arrest was observed in RIT.EGFP, Gag.MS2.SpCas9.TS, or Mock cultures.

Functional Knockout of Endogenous *CXCR4* by Gag.MS2.CRISPR/Cas9 All-in-One Particles

The chemokine receptor CXCR4 is a highly conserved molecule and is expressed on various cell types, including most hematopoietic cells (e.g., hematopoietic stem cells), Langerhans cells, vascular endothelial cells, neurons, and neuronal stem cells, as well as embryonic stem cells.[58] Studies described functionally expressed CXCR4 on the surface of various cancer cells, where it contributes to tumor growth, angiogenesis, and metastasis.[59] In addition to participation in embryonic development, cell proliferation, and migration, CXCR4 was shown to be the co-receptor of human CXCR4 (R4)-tropic HIV-1 strains.[60,61] During cell entry, the envelope glycoprotein of R4-tropic HIV-1 binds to the human CD4 and CXCR4 receptors, thereby initiating fusion of the viral lipid envelope with the host's cell membrane. Its involvement in diverse physiological processes and diseases, e.g., stem cell homing and HIV-1 infection, makes *CXCR4* an interesting target whose knockout may help to increase our understanding of the biological functions of CXCR4 in various cell types. Thus, we constructed CXCR4.TS.adj and CXCR4.TS.inc sgRNA expression plasmids (Figure 1D; Table S1) and generated *CXCR4*-targeting Gag.MS2.CRISPR/Cas9 all-in-one particles.[62] To show functional knockout of endogenous *CXCR4,* we sorted human Jurkat cells for similarly high CD4 and CXCR4 expression and transduced them with our Gag.MS2 particles (Figure 6A). Gag.MS2.CRISPR/Cas9 all-in-one particles targeting the murine *Tp53* gene (Table S1; Figure S8) served as a negative control, and an integrating LIT.CRISPR/Cas9.CXCR4 all-in-one vector served as a positive control (Figure 6B). Both CXCR4.TS.inc and CXCR4.TS.adj sgRNA-containing Gag.MS2.CRISPR/Cas9 all-in-one particles resulted in elevated levels of *CXCR4* knockout cells 5 days post-transduction (Figure 6C). However, although CXCR4.TS.adj and CXCR4.TS.inc displayed similar transfection efficiencies during particle production (data not shown), only Gag.MS2.CRISPR/Cas9.CXCR4.TS.adj all-in-one particles showed efficient and significant *CXCR4* knockout when compared to non-targeting Tp53 CRISPR/Cas9 particles. Due to the higher knockout rates, we thus proceeded with cultures that were treated with Gag.MS2.CRISPR/Cas9.CXCR4.TS.adj all-in-one particles. To validate our flow cytometry results with respect to DNA modification within the *CXCR4* gene locus, we performed a standard T7 endonuclease I assay (Figure 6D). Gag.MS2.CRISPR/Cas9 all-in-one-treated cultures revealed an average on-target *CXCR4* knockout efficiency of ~43%, which corresponds to ~71% knockout efficiency achieved with integrating LIT.CRISPR/Cas9.CXCR4 all-in-one vector particles (60.6%). To analyze the impact of *CXCR4* knockout on entry of R4-tropic HIV-1, we next transduced *CXCR4* knockout cultures with integrating CXCR4-tropic LIT.EGFP vector particles at MOI 0.2. We observed significantly impaired CXCR4-tropic LIT.EGFP transfer in Gag.MS2.CXCR4 knockout cultures compared to Gag.MS2.Tp53-treated control cultures (Figure 6E). The ratio of $EGFP^+/EGFP^-$ in $CXCR4^-$ cells revealed 4.3-fold reduced LIT.EGFP transfer in Gag.MS2.CRISPR/Cas9.CXCR4.TS.adj-treated knockout cultures. Furthermore, the same ratio calculated from $CXCR4^+$ cells showed impaired transduction with CXCR4-tropic LIT.EGFP. This suggests a mono-allelic knockout of *CXCR4* occurred in part of the cultures, which is supported by reduced CXCR4 mean fluorescent intensities (MFIs) in $CXCR4^+$-gated cells. Mono-allelic knockout of endogenous *CXCR4* was also observed in cultures that stably expressed the LIT.CRISPR/Cas9.CXCR4 all-in-one vector.

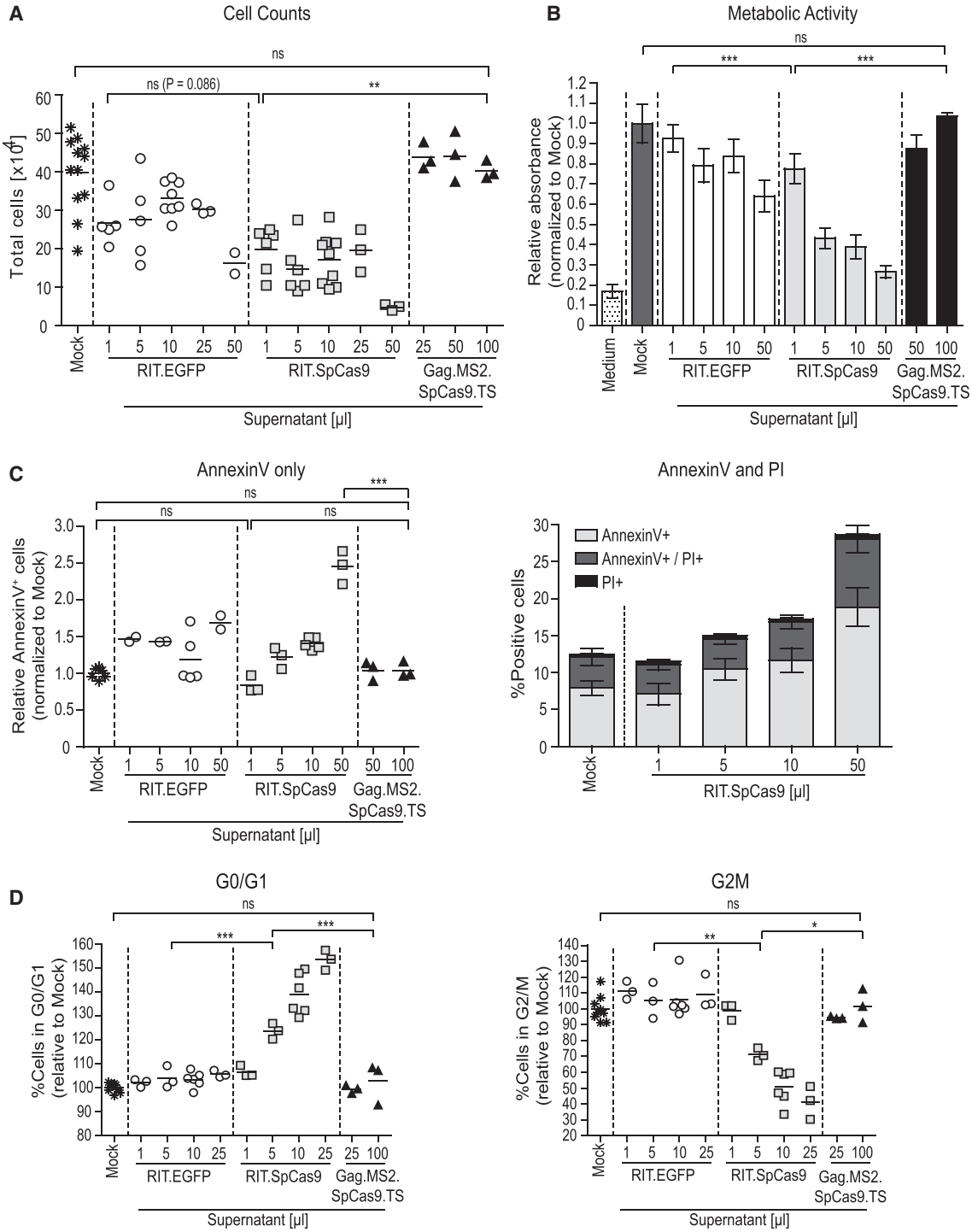

Figure 5. Stable and High-Dose SpCas9 Expression Is Cytotoxic

(A) Reduced cell numbers in RIT.SpCas9-treated cultures. NIH3T3 cells were transduced with integrating RIT.EGFP or RIT.SpCas9 particles or non-integrating Gag.MS2.SpCas9.TS particles. Based on titration via real-time qRT-PCR, RIT.EGFP and RIT.SpCas9 supernatants were adjusted before transduction (see also Figure S6D). Gag.MS2.SpCas9.TS supernatants were not adjusted. Cell counts were determined 4 days post-transduction. Non-treated NIH3T3 cells served as Mock control. (B) Prolonged and high-dose SpCas9 expression decreases the metabolic activity of NIH3T3 cells. To assess the metabolic activity, transduced cells of (A) were subjected to the colorimetric MTS cell proliferation and cytotoxicity assay. The graph shows the absorbance (490 nm) of purple formazan, which originated from the reduction of MTS by

(legend continued on next page)

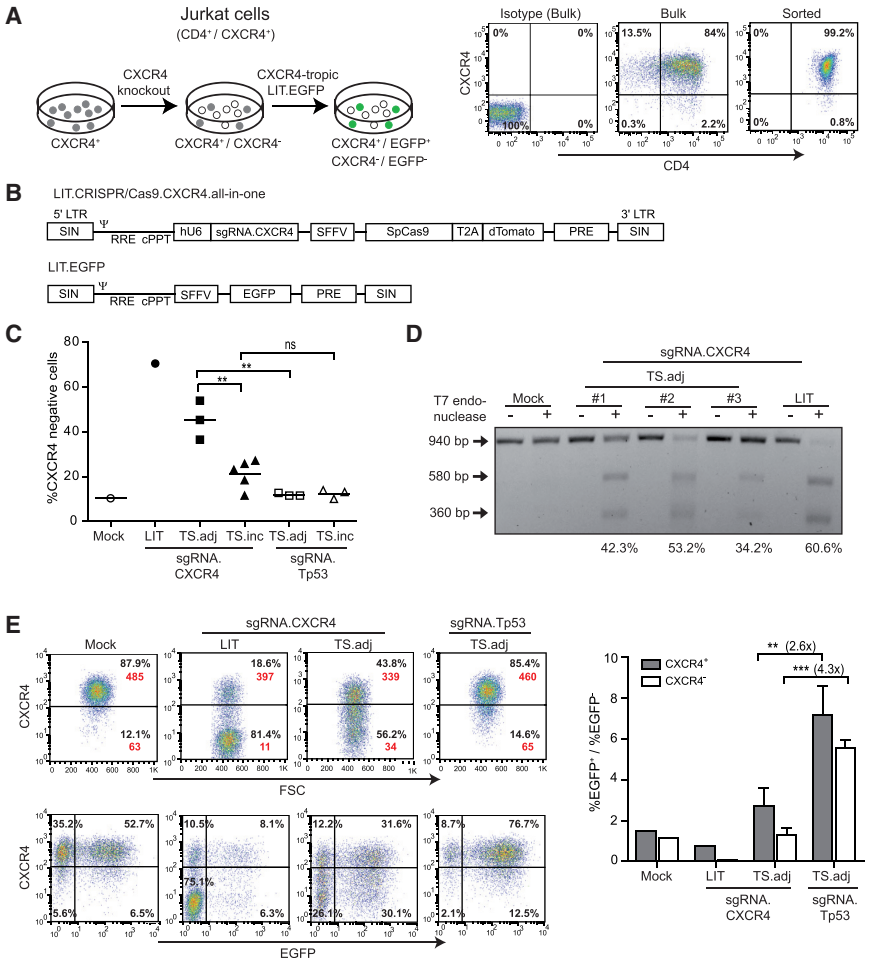

Figure 6. Functional Knockout of Endogenous *CXCR4* in Human Jurkat Cells

(A) Scheme of the functional *CXCR4* knockout experiment. Human Jurkat cells sorted for high CD4 and CXCR4 expression were transduced with LIT or Gag.MS2 CRISPR/Cas9 all-in-one particles for targeted *CXCR4* knockout. In a second round of transduction, *CXCR4* knockout cultures were transduced with a CXCR4-tropic LIT.EGFP vector. Only cells that still carry the CXCR4 receptor will be susceptible to transduction with CXCR4-tropic LIT.EGFP. The flow cytometric plots show CD4 and CXCR4 expression in Jurkat cells before and after sorting. (B) Schemes of LIT.CRISPR/Cas9.CXCR4 all-in-one and LIT.EGFP vectors. Depicted is the vector configuration after integration. All vectors are self-inactivating (SIN) due to deletion of viral enhancer and promoter sequences within the long terminal repeats (LTRs), and transgene expression (*SpCas9.P2A.dTomato* or *EGFP*) is driven by an internal spleen focus-forming virus (SFFV) promoter. In the LIT.CRISPR/Cas9.CXCR4 all-in-one vector, the hU6 promoter drives expression of sgRNA.CXCR4. Ψ, packaging signal; RRE, rev responsive element; cPPT, central polypurine tract; PRE, post-transcriptional regulatory element from woodchuck hepatitis virus. (C) Efficient *CXCR4* knockout by Gag.MS2.CRISPR/Cas9 all-in-one particles. Sorted $CD4^+/CXCR4^+$ Jurkat cells were transduced with LIT.CRISPR/Cas9.CXCR4 all-in-one particles (MOI 5) or either 25 μL of 100-fold concentrated (CXCR4.TS.inc and CXCR4.TS.adj) or 50 μL of 50-fold concentrated (Tp53.TS.inc and Tp53.TS.adj) Gag.MS2.CRISPR/Cas9 all-in-one particles. The knockout rate was determined by flow cytometry 5 days after transduction. Each data point reflects one independently generated supernatant. (D) Genome targeting efficiencies of LIT.CRISPR/Cas9.CXCR4 and Gag.MS2.CRISPR/Cas9.CXCR4.TS.adj all-in-one particles. The gDNA of *CXCR4* knockout cultures was subjected to a T7 endonuclease I assay. On-target activity is indicated by the cleavage of the 940 bp *CXCR4* PCR amplicon into 580 and 360 bp fragments. The InDel rate of each sample is depicted as a percentage. (E) Reduced CXCR4-tropic LIT.EGFP transduction rates in cultures that were treated with Gag.MS2.CRISPR/Cas9.CXCR4.TS.adj all-in-one particles. LIT.CRISPR/Cas9.CXCR4 all-in-one and Gag.MS2.CRISPR/Cas9.CXCR4.TS.adj cultures from (C) were individually transduced with CXCR4-tropic LIT.EGFP vector particles (9 days after CRISPR/Cas9 treatment). Three days later, cultures were analyzed by flow cytometry for EGFP and CXCR4 expression. The right graph depicts the ratios $EGFP^+/EGFP^-$ cells in $CXCR4^+$ or $CXCR4^-$ fractions expressed as mean ± SD. Representative flow cytometry plots are shown on the left (MFIs in red).

TP53 Knockout Endows Growth Advantage to Primary Human Fibroblasts

To test the feasibility of our non-integrating CRISPR/Cas9 all-in-one particles in primary cells, we aimed to knockout human *PTEN* and/or human *TP53* genes in primary NUFF cells, and knockout cells were directly compared to wild-type cells in competitive co-culture experiments (Figure 7). The *PTEN*-targeting sequence was derived from Cong et al.,[63] and we designed two protospacer sequences targeting *TP53*. The efficiency of the protospacer sequences targeting *PTEN* and *TP53* was validated using a fluorescent surrogate reporter cell line (Figure S8), and the PTEN and the best TP53 protospacer sequences (Table S1) were cloned into our non-viral sgRNA expression

cellular NAD(P)H. Results are shown as mean ± SD. (C) High-dose SpCas9 expression induces apoptosis. Transduced cells of (A) were co-stained with Annexin V and propidium iodide (PI) and analyzed for the occurrence of apoptotic (Annexin V^+) and dead (PI^+ or Annexin V^+/PI^+) cells. The left graph depicts the total percentage of Annexin V^+ cells in the respective samples. The right graph shows Annexin V^+, PI^+ and Annexin V^+/PI^+ cells of non-transduced Mock cells and cultures that were transduced with RIT.SpCas9. The error bars in the right graph indicate the SD of the mean. (D) High-dose SpCas9 expression resulted in a substantial G0/G1 cell-cycle arrest. NIH3T3 cells were freshly transduced with the depicted supernatants and volumes. Cultures were subjected to cell-cycle analysis 6 days post-transduction. The percentages of cells in G0/G1 and G2/M of transduced cultures were shown relative to the respective phase of non-transduced Mock cultures. Results depicted in (A)–(C) were generated with 2–3 independently packaged supernatants (RIT.EGFP = 2–3 supernatants, RIT.SpCas9 = 3 supernatants, and Gag.MS2.SpCas9.TS = 3 supernatants). Each data point presented in (D) was obtained from independently packaged supernatants (n = 3 biological replicates).

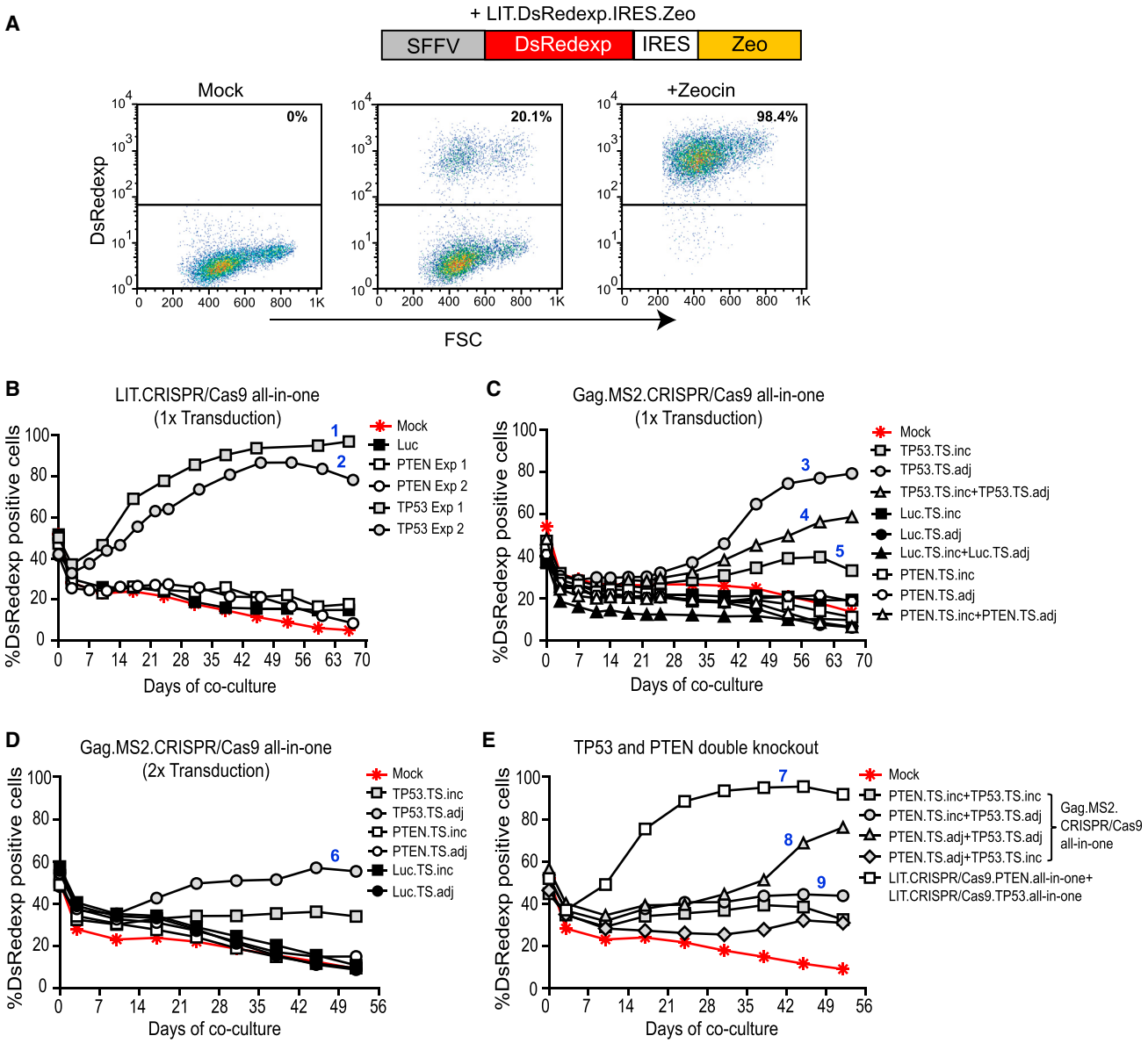

Figure 7. Growth Advantage of NUFF *TP53* Knockout Cells

(A) Generation of DsRedexp$^+$ NUFF cells. Freshly thawed NUFF cells (passage 9) were stably transduced with LIT.DsRedexp.IRES.Zeo encoding for *DsRedexp* and the *Zeocin* resistance gene (Zeo) at MOI 0.5. Co-expression of DsRedexp and Zeo was achieved by the internal ribosomal entry site (IRES) of endomycarditis virus and was initiated by enhancer and promoter sequences of SFFV. Transduced NUFF cells were selected with 100 μg/mL Zeocin for 10 days. The flow cytometric plots depict the percentage of DsRedexp$^+$ NUFF cells before and after Zeocin selection. (B) Knockout of *TP53*, but not *PTEN*, resulted in a growth advantage. DsRedexp$^+$ NUFF cells were transduced in a single round with LIT.CRISPR/Cas9 all-in-one vector particles for targeted knockout of *PTEN*, *TP53*, or Luc at MOI 10. Cells were mixed with non-treated wild-type NUFF cells 3 days post-transduction, and co-cultures were analyzed for DsRedexp expression for up to 67 days. The control co-culture of non-treated DsRedexp$^+$ and wild-type NUFF cells is marked in red. Exp 1, experiment 1; Exp 2, experiment 2. (C) Outgrowth of DsRedexp$^+$ NUFF cells that were treated with Gag.MS2.CRISPR/Cas9.TP53 all-in-one particles. DsRedexp$^+$ NUFF cells were transduced once with 50 μL of the depicted non-integrating Gag.MS2.CRISPR/Cas9 all-in-one particles. In TS.inc and TS.adj sgRNA combined samples, the respective supernatants were mixed at a ratio of 1:1 before transduction. (D) Transduction of DsRedexp$^+$ NUFF cells twice with Gag.MS2.CRISPR/Cas9.TP53 all-in-one particles slightly accelerates outgrowth of *TP53* knockout cells. The experiment was similar to that in (C), but DsRedexp$^+$ NUFF cells were transduced twice with Gag.MS2.CRISPR/Cas9 all-in-one particles on 2 consecutive days before co-culture. (E) Double knockout of *PTEN* and *TP53* by Gag.MS2.CRISPR/Cas9 all-in-one particles did not accelerate outgrowth of DsRedexp$^+$ NUFF cells. Before co-culture, DsRedexp$^+$ NUFF cells were co-transduced with either LIT or Gag.MS2 CRISPR/Cas9 all-in-one particles targeting *TP53* or *PTEN*. LIT.CRISPR/Cas9 all-in-one supernatants were each applied at MOI 10, and 50 μL of each Gag.MS2.CRISPR/Cas9 all-in-one supernatant was used. The curves were obtained from individual transductions with independently generated supernatants. Numbers 1–9 (in blue) displayed in graphs (B)–(E) indicate selected cultures that were expanded for gDNA harvest and subjected to InDel analyses (see also Tables S2–S5).

constructs (Figure 1D). The performance of wild-type and TS-containing sgRNAs was validated by the T7 endonuclease I assay after transfecting the plasmids into HT1080-based RFP657.Tet2+SpCas9 reporter cells (Figure S9). The results confirmed efficient *PTEN* and *TP53* cleavage and revealed no obvious differences among the different sgRNA backbones. In addition, we inserted protospacers targeting *PTEN* or *TP53* into integrating LIT.CRISPR/Cas9 all-in-one vectors,[56] which served as positive controls (Figure S10A). An sgRNA targeting the *Renilla luciferase* (Luc) gene was co-packaged as non-specific control. Because our MLV-based Gag.MS2 chimeras are transient and therefore do not permanently label transduced cells, we conducted a competitive culture experiment with wild-type and red-fluorescent CRISPR/Cas9-treated NUFF cells. In this experiment, freshly thawed primary NUFF cells were transduced with integrating LIT.DsRedexp.IRES.Zeo particles (MOI 0.5), which expresses *DsRedexp* and the *Zeocin* resistance gene (Figure 7A). After enrichment of cells with Zeocin to ~98% DsRedexp positivity, we transduced these cultures with transient Gag.MS2 or integrating LIT.CRISPR/Cas9 all-in-one particles (Figures 7B–7E). In total, three experimental settings were chosen: (1) DsRedexp$^+$ NUFF cells were treated once (Figures 7B and 7C) or (2) twice (only Gag.MS2 particles) (Figure 7D) with CRISPR/Cas9 all-in-one particles targeting either *PTEN* or *TP53*, or (3) *PTEN* and *TP53* were targeted simultaneously (Figure 7E). Subsequently, transduced DsRedexp$^+$ NUFF cells were co-cultured with wild-type NUFF cells at a ratio of 1:1 and closely monitored up to 67 days. Only knockout of *TP53*, not *PTEN*, promoted outgrowth of DsRedexp$^+$ NUFF cells in co-cultures with stable LIT.CRISPR/Cas9 all-in-one expression (Figure 7B). However, analyses of respective mono-cultures showed stable long-term expression of LIT.CRISPR/Cas9 all-in-one vectors (Figure S10B) and efficient targeted knockout of both *PTEN* and *TP53* genes (Figure S10C), thus excluding vector silencing and/or a non-functional PTEN sgRNA as the underlying mechanism for the observed phenotype. Strikingly, even single treatment with non-integrating Gag.MS2.CRISPR/Cas9.TP53 all-in-one particles (Figure 7C) conferred a growth advantage to DsRedexp$^+$ NUFF cells compared to treatment with PTEN or Luc Gag.MS2.CRISPR/Cas9 all-in-one knockout particles. Interestingly, the outgrowth of *TP53* knockout cells was delayed in non-integrating Gag.MS2 compared to integrating LIT.CRISPR/Cas9 *TP53* knockout cultures (compare graphs in Figures 7B and 7C). Whereas the growth advantage of LIT.CRISPR/Cas9.TP53-treated cells became clearly visible within 10 days of co-culture, outgrowth of Gag.MS2.CRISPR/Cas9.TP53.TS.adj- or TP53.TS.inc-treated cells was observed only ~3 weeks later. Double transduction of DsRedexp$^+$ NUFF cells with Gag.MS2.CRISPR/Cas9.TP53 knockout particles shortened clonal outgrowth kinetics by ~2 weeks (Figure 7D). These data suggest that Gag.MS2.CRISPR/Cas9 all-in-one particles exhibit a lower efficacy, which is expected, because they deliver *SpCas9* and the sgRNA in a transient (hit-and-run) fashion, whereas stably integrated LIT vectors mediate high and constitutive CRISPR/Cas9 component expression. High and prolonged CRISPR/Cas9 component overexpression is likely to be associated with off-target effects,[21,64,65] thereby inducing potential second and/or multiple oncogenic hits, which might have also contributed to the increased outgrowth kinetics of LIT.CRISPR/Cas9.TP53 knockout cultures.[66,67] To check whether a combined knockout of *PTEN* and *TP53* would also increase clonal outgrowth, we co-transduced DsRedexp$^+$ NUFF cells with PTEN and TP53 Gag.MS2 or LIT CRISPR/Cas9 all-in-one knockout particles. For both particle types, co-transduction conferred a growth advantage but did not alter outgrowth kinetics of transduced DsRedexp$^+$ NUFF cells (Figure 7E). Finally, we expanded selected wells at the endpoint of our co-culture experiments and analyzed the cultures for the occurrence of InDels (blue numbers 1–9 in Figures 7B–7E). We amplified the respective gene loci (*TP53* and/or *PTEN*), cloned the PCR fragments into a shuttle vector, transformed them into bacteria, and sequenced plasmid DNA of up to 20 bacterial clones. In *TP53* knockout cultures, we found InDels for integrating and non-integrating CRISPR/Cas9 all-in-one particles (Tables S2–S5). The number and variety of InDels correlated with the percentage of DsRedexp$^+$ NUFF cells in these expanded co-cultures. Integrating and non-integrating CRISPR/Cas9 co-cultures with similar amounts of DsRedexp$^+$ cells did not reveal clear differences regarding InDel frequency and/or heterogeneity. Deletion of a single G 4 bp upstream of the TGG PAM motif results in a premature stop codon and was found at higher frequencies in co-culture samples from different experiments, suggesting a more potent dominant negative TP53 mutation that supported the outgrowth of the cells. Sequence analyses of outgrown cultures that were co-transduced with either integrating or non-integrating CRISPR/Cas9 PTEN and TP53 knockout particles revealed on-target knockout for *TP53* for both particle types, but InDel formation in *PTEN* was only observed with stably integrating LIT.CRISPR/Cas9.PTEN all-in-one particles. These results argue for a greater selective advantage of NUFF cells with a mutated *TP53* gene and explain the unchanged outgrowth kinetics of transduced DsRedexp$^+$ NUFF cells depicted in Figure 7E.

DISCUSSION

Safe and transient expression of DNA-modifying technologies is a long-standing challenge and a prerequisite for human gene and cell therapies. Thus, the development of efficient and non-cytotoxic delivery methods for short-term expression of gene editing molecules is of great interest. In this study, we established non-integrating MLV-based CRISPR/Cas9 all-in-one particles for targeted gene knockout. Stepwise validation of this technique allowed us to develop a highly efficient tool to co-deliver *SpCas9* and sgRNAs targeting different genes into target cells. Both CRISPR/Cas9 components were provided as non-viral RNA transcripts embedded within virus-like particles that follow the cellular entry route of retroviruses. Specific packaging of *SpCas9* mRNA and Pol III-derived sgRNA transcripts was achieved by redirection of the highly conserved retroviral packaging mechanism. We successfully edited various murine and human cell lines, as well as primary human fibroblasts, with our system. We showed efficient disruption of the surrogate RFP657.Tet2 reporter gene, as well as targeted and functional knockout of endogenous *CXCR4* and *TP53* genes. Comparison of two positions of the MS2 TS hairpin dimer (TS.inc versus TS.adj) demonstrated better knockout efficiencies for Gag.MS2.CRISPR/Cas9 all-in-one particles that

contain the TS.adj sgRNA variant. Finally, we found that stable and high-dose expression of the SpCas9 enzyme is cytotoxic. In contrast to EGFP, continuous SpCas9 expression triggered a G0/G1 cell-cycle arrest, which was associated in particular with reduced cell numbers and restricted metabolic activity. None of these cytotoxic side effects were observed for transiently expressed SpCas9, as achieved by the technology presented here.

Upon validation of our technique, we observed efficient *RFP657* knockout after transient delivery of *SpCas9.TS* mRNA into mouse and human RFP657.Tet2+sgRNA.Tet2 reporter cells (Figures 2A and S3A). In contrast, individual transfer of sgRNA.TS variants via Gag.MS2 particles into the SpCas9-expressing RFP657.Tet2 reporters was far less efficient (Figures 2B and S3B). These observations suggest that the bottleneck of CRISPR/Cas9-mediated gene knockout with our Gag.MS2 particles is functional delivery of the sgRNA.TS rather than the *SpCas9.TS* mRNA transcript. One reason for the poor performance of Gag.MS2.sgRNA.TS particles might be the shorter half-life of the Pol III-driven, uncapped, and non-polyadenylated sgRNA transcripts in target cells. Recent reports showed enhanced genome editing when providing SpCas9, together with chemically modified and stabilized guide RNAs.[25,68] In line with this, direct comparison of Tet2.TS.adj and Tet2.TS.inc individual delivery into murine or human RFP657.Tet2+SpCas9 reporter cells revealed higher knockout rates for Tet2.TS.adj particles (Figures 2B and S3B). The observed 2-fold lower Tet2.TS.adj content in individual particles compared to Tet2.TS.inc (Figure 4B) suggests that positioning of the two MS2 TS hairpins 3′ of the sgRNA scaffold might enhance sgRNA stability and/or effectivity. In contrast to our findings, another study found that TS.inc exhibited higher activity than the corresponding TS.adj sgRNA construct when used with a CRISPR/Cas9 complex engineered for transcriptional activation of endogenous genes.[54] Differences between the two studies might be explained by the nature of the two methodologies (gene editing versus gene regulation) and/or that our TS.adj sgRNA variant has a slightly different design in terms of the length and base pairs of the TS hairpin linker and spacer sequences. In contrast to individual Gag.MS2.Tet2.TS particles described earlier, Gag.MS2.CRISPR/Cas9 all-in-one particles showed an inverted ratio and 2-fold better packaging of Tet2.TS.adj compared to Tet2.TS.inc sgRNAs (compare Figure 4B and Table 1). Because Gag.MS2.CRISPR/Cas9 all-in-one particles contain SpCas9 protein, in addition to *SpCas9* mRNA, one could speculate that the observed differences in sgRNA abundance can be explained by more efficient binding of SpCas9 protein to Tet2.TS.adj and the resultant unspecific incorporation of these RNP complexes into our Gag.MS2.CRISPR/Cas9 all-in-one particles.

In addition to SpCas9 proteins, molecular characterization of our Gag.MS2 particles revealed the presence of CRISPR/Cas9 RNA transcripts that lack TS sequences (Figure 4), although to a clearly lesser extent than transcripts harboring TS. This observation is in accordance with current literature on the packaging of host RNAs and proteins into wild-type retroviruses and retroviral vectors, where up to 30% of RNAs within retroviral virions originate from the host, with a preference for small RNAs.[39,69–71] Potential disadvantages of this phenomenon include unintended transfer of cellular RNAs and bioactive proteins, as well as induction of immunogenicity. Improved characterization of the constituents of viral vector particles may allow safer clinical use of these gene therapy products.

Our observation that knockout efficiencies were higher with all-in-one particles versus co-transduction of SpCas9.TS and sgRNA.TS Gag.MS2 particles (Figures 2C, 3, S3C, S4C, and S4D) may be explained by the following, possibly interconnected, reasons: (1) Co-packaging facilitates correct spatiotemporal delivery of *SpCas9.TS* and sgRNA.TS transcripts and/or efficient generation of the SpCas9/sgRNA RNP complex, and (2) the shorter half-life of the small, non-capped, and non-polyadenylated sgRNAs (compared to the *SpCas9* mRNA) restricts RNP complex formation after individual delivery of both components. Reports showed that the Cas9 protein is essential for guide RNA stability in living cells and that guide RNAs are significantly protected from degradation by cellular endo- and exonucleases once they are loaded into the CRISPR/Cas9 RNP complex.[25,72] Thus, one could envision that co-delivery of both RNA transcripts close within the same Gag.MS2 particle results in immediate loading of sgRNA.TS into a protective and stable CRISPR/Cas9 RNP complex as soon as translation of *SpCas9.TS* mRNA has occurred.

To our knowledge, this is the first report of a dose-dependent cytotoxicity of the SpCas9 enzyme (Figure 5). Continuous and high-dose SpCas9 expression in the absence of an sgRNA resulted in a substantial G0/G1 cell-cycle arrest in NIH3T3 cells. In contrast to stable EGFP expression, more pronounced reductions in cell growth and metabolic activity were detectable at MOI 13 (1 μL supernatant), whereas the significant G0/G1 arrest was first observed at MOI > 13. In addition, cell death and/or apoptosis within transduced cultures were only significantly increased at even higher MOIs. This suggests that SpCas9 expression can be tolerated by cells to a certain degree, which is consistent with the viability of ubiquitously expressing SpCas9 transgenic mice.[73] However, reduced cell numbers and reduced metabolic activity without overt G0/G1 arrest and/or cell death observed at MOI 13 imply that the cell physiology is affected by prolonged SpCas9 expression, which presumably results in deceleration of the cell cycle at a moderate dose and manifests as G0/G1 arrest upon high-dose stable SpCas9 expression. Furthermore, because HDR takes place in S and G2 phases, a prolonged G0/G1 phase or a G0/G1 cell-cycle arrest will result in lower efficiency of CRISPR/Cas9-mediated HDR. Thus, in addition to the natural limitations of HDR,[74] such as its competition with NHEJ in S/G2, overly high SpCas9 expression in target cells could be an additional explanation for the relatively low CRISPR/Cas9-mediated HDR efficiencies compared to NHEJ-based gene knockout strategies.[75] This is supported by studies in which temporal expression of SpCas9 in S, G2, and M phases improved CRISPR/Cas9-mediated HDR efficiency.[76,77]

The Achilles' heel of DNA-modifying enzymes are cyto- and genotoxic side effects,[17–20] which are particularly unwanted in human

gene and cell therapies. Several studies showed that plasmid-based delivery methods of CRISPR/Cas9 components suffer from off-target events and/or unwanted integration of DNA segments derived from the transfected Cas9 and guide RNA-encoding plasmids.[21,25,65,78] Short-term and dose-controlled co-transfer of Cas9 as purified protein or *in vitro* transcribed mRNA and the respective guide RNA—as part of a hit-and-run strategy—clearly reduced the incidence of off-target events when compared to plasmid DNA transfection.[21,22,25] Conventionally, Cas9 protein and guide RNA RNP complexes, or alternatively, Cas9-encoding mRNA and guide RNA transcripts, are electroporated or introduced via lipofection into cells. Each of these techniques delivers guide RNA and Cas9 in huge excess, and the delivery mode can contribute to cytotoxicity and/or exhibit low efficiency, especially in primary cells.[79,80] The approach presented here exploits evolutionary conserved retroviral entry mechanisms and cellular host proteins as partners. This is usually well tolerated by target cells and not associated with voltage-induced cytotoxicity as still observed for electroporation-assisted delivery strategies to introduce CRISPR/Cas9 RNA and/or protein components.[28,81,82] The possibility to use novel pseudotyping glycoproteins makes it possible to confine delivery of our chimeric Gag.MS2 particles to specific cell types, as described for retroviral targeting strategies by Buchholz and co-workers.[83–85] Calculation of amounts of Cas9 (in either mRNA or protein form) and guide RNA administered for gene editing in recently published articles led to estimates in the range of 1–15 pg mRNA/cell (i.e., 4.2×10^5–6.3×10^6 mRNA molecules/cell), 5–75 pg Cas9 protein/cell (i.e., 1.8×10^7–2.8×10^8 protein molecules/cell), and 1–100 pg guide RNA/cell (i.e., 1.9×10^7–1.9×10^{10} guide RNA molecules/cell).[21,22,25,68,86] Based on data presented in Table 1 and an average *RFP657* knockout efficiency of 44%–56%, we calculated that 9.6×10^2–3.8×10^3 *SpCas9.TS* mRNA molecules/cell and 7.1×10^4–5.8×10^5 sgRNAs/cell were delivered (to 1×10^5 cells with 50 µL of our 100-fold concentrated Gag.MS2 particles). This is substantially lower than the amount of *SpCas9* mRNA and guide RNA molecules used in conventional CRISPR/Cas9 RNA electroporation protocols. In addition, ~0.2 pg SpCas9 protein/cell was transferred. Thus, the targeted and exploited retroviral entry route and, in the case of Gag.MS2.CRISPR/Cas9 all-in-one particles, better spatiotemporal co-delivery of *SpCas9* mRNA and sgRNA make our delivery method more efficient. In addition, Gag.MS2.CRISPR/Cas9 all-in-one particles likely deliver SpCas9/sgRNA RNP complexes, in addition to *SpCas9* mRNA and sgRNA (Figures 4C and 4D).

In conclusion, the Gag.MS2 chimeras introduced here represent an alternative technology for transient, high-efficiency, and non-toxic transfer of CRISPR/Cas9 components into target cells. Co-packaging of *SpCas9* mRNA and sgRNA transcripts into MLV-derived Gag.MS2 particles ensures their spatiotemporal co-delivery and allows for potential targeting of these particles to various cell types via novel pseudotyping strategies.[83] Finally, optimization of *SpCas9* mRNA and sgRNA packaging and/or stability (e.g., incorporation of >2 MS2 TS hairpins and/or RNA stabilizing motifs),[87,88] as well as improved uncoating strategies of incoming Gag.MS2 particles,[89] may enhance this technology.

MATERIALS AND METHODS

Vector Design

The cloning strategies of all retroviral and non-viral expression plasmids that were used in this study are described in detail in Supplemental Materials and Methods.

Cell Culture

HEK293T, human HT1080, murine NIH3T3, murine SC-1 cells, and their derivatives were cultured in DMEM (Biochrom, Berlin, Germany) with 10% heat-inactivated fetal bovine serum (FBS) (PAN Biotech, Aidenbach, Germany), 100 U/mL penicillin, 100 µg/mL streptomycin, and 1 mM sodium pyruvate (all from PAA, Coelbe, Germany). In the case of human and murine RFP657.Tet2 and RFP657.Tet2+sgRNA.Tet2 reporter cells, DMEM was supplemented with 1.5 µg/mL puromycin (InvivoGen, Toulouse, France). Murine and human RFP657.Tet2+SpCas9 reporter cells were cultured in the presence of 1.5 µg/mL puromycin and 20 µg/mL blasticidin (InvivoGen). Human Jurkat cells were cultured in RPMI medium 1640 (PAN Biotech) supplemented with 10% FBS, 100 U/mL penicillin, 100 µg/mL streptomycin, and 1 mM sodium pyruvate. Primary NUFF cells were purchased (passage 9 after isolation from healthy donors; Amsbio, Abingdon, United Kingdom) and cultivated in DMEM low glucose (PAN Biotech) supplemented with 15% heat-inactivated FBS, 100 U/mL penicillin, 100 µg/mL streptomycin, 2 mM L-glutamine (Biochrom), 1% minimal essential medium (MEM) nonessential amino acids solution (Gibco/Thermo Fisher Scientific, Schwerte, Germany) and 100 µM β-mercaptoethanol (Sigma-Aldrich, Munich, Germany).

Production of Integrating Retroviral and Transient Gag.MS2 Vector Particles

Retroviral and Gag.MS2 vector particles were produced by transient transfection of HEK293T cells via the calcium phosphate precipitation method as previously described.[90] 5×10^6–6×10^6 HEK293T cells were seeded in a 10 cm dish the day before transfection. On the day of transfection, the DMEM was replaced by transfection medium composed of DMEM supplemented with 20 mM HEPES (PAN Biotech) and 25 µM chloroquine (Sigma-Aldrich). To produce VSVg-pseudotyped LIT vector particles, 5 µg of the lentiviral vector expression plasmid was co-transfected with 12 µg lentiviral wild-type Gag-Pol (G/P) (pcDNA3.HIV-1.G/P.4 × CTE),[91] 5 µg Rev (pRSV.Rev; provided by T. Hope, Northwestern University, Chicago, IL, USA), and 2 µg VSVg (pMD.G).[92] The integrating R4-tropic, EGFP-expressing LIT.EGFP vector particles were generated by co-transfection of 10 µg pLeGO-G2 vector plasmid,[93] 10 µg pMDLg/pRRE (HIV-1 G/P),[94] 5 µg pRSV.Rev, and 4 µg phCMV.HIVenv.NL4-3 (R4-tropic envelope) expression plasmids. RIT vector preparations were generated with 5 µg vector plasmid, 7 µg pcDNA3.MLV.G/P,[91] and 2 µg pMD.G. Non-integrating MLV-based Gag.MS2 particles delivering *SpCas9* mRNA or sgRNA were produced with 5 µg pMS2.Gag, 2 µg pMLV.Pol.only, 2 µg pMD.G, and

either non-viral SpCas9 or sgRNA expression plasmids, respectively. The generation of Gag.MS2.CRISPR/Cas9 all-in-one particles was accomplished with 5 μg pGag.MS2, 2 μg pMLV.Pol.only, 2 μg pMD.G, and 5 μg each of the respective sgRNA and SpCas9 expression plasmids. The transfection efficiencies of all Gag.MS2 particle productions were determined by fluorescence-activated cell sorting (FACS) analysis. If not indicated otherwise, all VSVg-pseudotyped supernatants were concentrated 50-fold via ultracentrifugation either overnight at 13,238 × *g* (4°C) or at 82,740 × *g* (4°C) for 90–120 min. The CXCR4-tropic LIT.EGFP supernatants were not concentrated.

Transduction of Cells with Retroviral and Gag.MS2 Supernatants

Functional titers of integrating retroviral vectors were determined by transduction of murine (RIT vectors) or human (LIT vectors) cell lines with serial dilutions of the respective supernatant. The day before transduction, 5×10^4 HT1080, NIH3T3, or SC-1 cells were seeded per well of a 12-well plate. The next day, different volumes of the respective supernatants and volumes were applied to the cells. Two to three days later, the cells were harvested and analyzed by flow cytometry. For titer determination, only transduction efficiencies of 5%–30% were used. The transduction of all CRISPR/Cas9 reporter cells with Gag.MS2 particles followed the titration protocol described earlier. However, supernatants were used at the given volumes, and *RFP657* knockout rates were determined by flow cytometry 5–6 days post-transduction. For knockout of human endogenous *CXCR4*, 2×10^5 Jurkat cells, previously sorted for high CD4 and CXCR4 expression, were seeded per well of a 24-well-plate and transduced with LIT.CRISPR/Cas9.CXCR4 all-in-one particles at MOI 5 or 50 μL of the respective Gag.MS2.CRISPR/Cas9 all-in-one particles. FACS-based *CXCR4* knockout analysis was conducted 5 days post-transduction. Subsequently, 2×10^5 cells of each *CXCR4* knockout culture were transduced with CXCR4-tropic LIT.EGFP at MOI 0.2. Three days later, the percentages of $EGFP^+$ cells in $CXCR4^+$ and $CXCR4^-$ populations was measured via flow cytometric analysis. $DsRedexp^+$ and Zeocin-resistant NUFF cells were generated by transduction of 1×10^5 freshly thawed NUFF cells (passage 9; Amsbio) with LIT.DsRedexp.IRES.Zeo (MOI 0.5) and subsequent selection with 100 μg/mL Zeocin (Invitrogen/Thermo Fisher Scientific) for 11 days. For knockout of endogenous *TP53* and/or *PTEN* genes in $DsRedexp^+$ NUFF cells, 5×10^4 cells were seeded per well of a 12-well plate. The following day, the cells were transduced with respective integrating LIT.CRISPR/Cas9 all-in-one (MOI 10) or Gag.MS2.CRISPR/Cas9 all-in-one (50 μL) supernatants. Flow cytometric analyses of transduced mono-cultures or competitive co-cultures were performed at the given time points. All transductions described in this section were assisted by 4 μg/mL protamine sulfate (Sigma-Aldrich) and centrifugation at 400 × *g* and 37°C for 1 hr.

Analysis of Gag.MS2 Particles Delivering *SpCas9* mRNA and Guide RNA

Integrating RIT and transient Gag.MS2 CRISPR/Cas9.Tet2 all-in-one particles were generated as described earlier. However, supernatants were concentrated 100-fold, and the particles were resuspended in PBS buffered with 20 mM HEPES. For the detection of residual integration events (Figure 4E), we transduced 1×10^6 HT1080 cells with 30 μL of the depicted concentrated supernatants. Non-transduced Mock cells served as negative control. As described earlier, transduction was supported by 4 μg/mL protamine sulfate and centrifugation at 400 × *g* and 37°C for 1 hr. After centrifugation, the plates were transferred to the incubator (37°C/5% CO_2) for 1 hr. Then, the cells were liberated from the particle-containing transduction medium, washed twice with 2 mL of warm PBS, fed with 2 mL fresh DMEM, and placed back to the incubator. Cell samples were harvested 10 days post-transduction to prepare gDNA with the QIAamp DNA Blood Mini Kit (QIAGEN, Hilden, Germany) following the manufacturer's instructions. To determine the CRISPR/Cas9 RNA content within RIT and Gag.MS2 supernatants (Figures 4A and 4B; Table 1), supernatants were first liberated from plasmid and gDNA contaminations by treatment with TURBO DNase (Invitrogen/Thermo Fisher Scientific). Particle RNA was then isolated using the QIAGEN RNAeasy Micro Kit. To control for equal column elution efficiency, a defined amount of a RIT.Cre supernatant was added. cDNA was prepared via the QuantiTect Reverse Transcription Kit from QIAGEN. Quantitative real-time PCRs of cDNA and gDNA were conducted on an Applied Biosystems StepOnePlus Real-Time PCR System (Thermo Fisher Scientific) using the QuantiTect Sybr Green PCR Kit (QIAGEN). Non-reverse transcribed RNA samples served as control for successful plasmid and gDNA elimination. CRISPR/Cas9 RNA transcripts and residual integration events of Gag.MS2.CRISPR/Cas9 all-in-one particles were detected with primers 5′-GAGGAGTTGTGGCCCGTGT-3′ and 5′-TGACAG GTGGTGGCAATGCC-3′ (PRE element), as well as 5′-GAACAA GCTCTACATCCCGTGT-3′ and 5′-CAAGTTGATAACGGACTAG CCTT-3′ (Tet2 sgRNA). Signals were normalized to either the signal obtained by the amplification of human beta-actin cDNA (RNA origin) or the signal obtained by the amplification of a conserved intron of the polypyrimidine tract binding protein (PTBP2).[17,90] Quantitative real-time PCR data were analyzed with the StepOneSoftware v.2.3 program (Thermo Fisher Scientific). RNA results were quantified using the comparative threshold cycle method.[95] Calculation of integrated mean VCNs and CRISPR/Cas9 transcripts was performed with the help of plasmid standards containing the respective target sequences.

For western blot analysis, 10 μL of the respective supernatants were mixed with 10 μL of Laemmli buffer and denatured at 95°C for 5 min. Subsequently, 15 μL of the supernatant lysates were separated by an SDS-PAGE (12.5% gel) and transferred to a nitrocellulose membrane (GE Healthcare Life Science, Solingen, Germany). After staining all blotted proteins with Ponceau S (Sigma-Aldrich), the membrane was successively probed with a rabbit polyclonal anti-enterobacteriophage MS2 coat protein antibody (1:5,000) (Merck Millipore, Darmstadt, Germany) and a monoclonal mouse purified anti-CRISPR (Cas9) antibody (1:1,500) (BioLegend, Koblenz, Germany) in Tris-buffered saline with 0.05% Tween and 3% milk powder at 4°C overnight (both Roth, Karlsruhe, Germany). Horseradish peroxidase-conjugated goat anti-rabbit immunoglobulin G (IgG) (1:2,000) or goat anti-mouse IgG (1:2,000) secondary antibodies

were used (both Santa Cruz Biotechnology, Heidelberg, Germany). Protein signals were visualized by treating the membranes with SuperSignal West Pico chemiluminescent substrate (Thermo Fisher Scientific), and the obtained signals were detected and analyzed with the Fusion imaging system (Vilber Lourmat, Eberhardzell, Germany). SpCas9 protein content in Gag.MS2 particles was measured by the EpiQuik CRISPR/Cas9 Assay ELISA Kit (Epigentek Group, Farmingdale, NY, USA) following the manufacturer's instructions. The absorbance was measured at 490 and 655 nm using an ELISA plate reader SpectraMax 340PC (Molecular Devices, Biberach, Germany).

Cytotoxicity Assays

As described in Supplemental Materials and Methods, integrating RIT.EGFP, RIT.SpCas9.P2A.EGFP (RIT.SpCas9), and non-integrating Gag.MS2.SpCas9.P2A.EGFP.TS (Gag.MS2.SpCas9.TS) supernatants were titrated via real-time qRT-PCR based on cytoplasmic vector RNA levels 3 hr after particle application. Consequently, RIT.EGFP and RIT.SpCas9 supernatants were adjusted and used to transduce 1×10^5 NIH3T3 cells with the displayed volumes. Gag.MS2.SpCas9.TS supernatants were not adjusted, because their adjustment would have exceeded applicable volumes of supernatant. The cells were harvested 4 days post-transduction and counted, and 2×10^3 or 2×10^4 cells were seeded per well of a 96- or 12-well plate, respectively. After another 3 days, cells that were seeded in a 96-well plate were analyzed for metabolic activity using the CellTiter 96 AQ_{ueous} One Solution Cell Proliferation Assay (3-(4,5-dimethyl-2-yl)-5-(3-carboxymethoxyphenyl)-2-(4-sulfophenyl)-2H-tetrazolium, inner salt [MTS] assay; Promega, Madison, WI, USA) according to the manufacturer's protocol. One day later, cells from 12-well plates were analyzed for apoptosis by co-staining the cultures with allophycocyanin (APC) Annexin V (BD Biosciences Clontech) and PI (Sigma-Aldrich). For cell-cycle analyses, 5×10^4 freshly transduced NIH3T3 cells were seeded per well of a 12-well plate (day 3 post-transduction). The cells were harvested 6 days after transduction, counted, and subjected to cell-cycle analysis. 5×10^4 cells were washed with PBS (PAN Biotech), resuspended in 100 µL PI staining buffer—10 mM Tris-HCL [pH 7.4] (Tris-Base, Biomol, Hamburg, Germany; HCL, Roth), 0.1% Triton X-100 (Sigma-Aldrich), and 5 mM $MgCl_2$ (Roth) supplemented with 15 µg/mL RNase A (QIAGEN) and 50 µg/mL PI—and incubated for 30 min at 4°C in the dark. Before flow cytometry, 500 µL FACS buffer (PBS containing 2% heat-inactivated FBS) was added per sample.

T7 Endonuclease I Assay and Sequencing of InDels

gDNA of CRISPR/Cas9-treated cells was isolated with QIAamp DNA Blood Mini Kit (QIAGEN) following the manufacturer's protocol. Targeted gene loci were amplified with oligonucleotide primers 5′-ACTTCAGATAACTACACCGAGG-3′ and 5′-CAGCACGCAC TCACCTCTGTG-3′ (*CXCR4*; 940 bp amplicon), 5′-GTACCAGA TAATTATTTCATCG-3′ and 5′-CTCATGTTACAATGCCATA AG-3′ (*PTEN*; 746 bp amplicon), or 5′-GGAGCCGCAGTCAGA TCCTAG-3′ and 5′-GCTGAGGGTGTGATGGGATG-3′ (*TP53*; 821 bp amplicon). All PCR products were purified by agarose gel electrophoresis and extracted from the gel using the QIAquick Gel Extraction Kit (QIAGEN). For the T7 endonuclease I assay, 200 ng of the PCR product was denatured and reannealed using the following program: denaturation at 95°C for 5 min, ramp down to 85°C at 2°C/s, ramp down to 22°C at 0.1°C/s, and hold at 4°C. Next, the volume of the samples was equally divided in 2 parts. One part was incubated with 10 U/µL T7 endonuclease I (New England Biolabs, Frankfurt, Germany), and the other part was incubated with the respective volume of H_2O for 20 min at 37°C. After incubation, the reactions were separated by agarose gel electrophoresis, and on-target knockout efficiencies were calculated with the previously published formula: $\%InDel = 100 \times (1 - (1 - \text{fraction cleaved})^{0.5})$.[96] For InDel sequencing (Figures 7 and S10; Tables S2–S5), the PCR products were subcloned into a shuttle vector, and the resulting plasmids were transformed into XL1-blue bacteria (Agilent, Waldbronn, Germany). Depending on the sample, plasmid DNA of 6, 10, or 20 bacterial clones was subjected to Sanger sequencing (Microsynth Seqlab, Göttingen, Germany).

Statistical Analysis

Data from experiments are expressed as means or means ± SD. For statistical comparison of two groups in graphs from Figures 2 and 6 and Figures S2A, S3, and S5, we performed an unpaired two-tailed t test. Data from Figures 3 and 5 and Figures S2B and S2C were analyzed by using one-way ANOVA, together with Tukey's multiple comparison post hoc tests. Values of $p > 0.05$ were considered not significant (NS), and values of $^*p \leq 0.05$ were considered significant, $^{**}p \leq 0.01$ were considered very significant, and $^{***}p \leq 0.001$ were considered extremely significant. The sample size (n) for each experiment is mentioned in the respective figure legend.

SUPPLEMENTAL INFORMATION

Supplemental Information includes Supplemental Materials and Methods, ten figures, and five tables and can be found with this article online at https://doi.org/10.1016/j.omtn.2018.09.006.

AUTHOR CONTRIBUTIONS

Conceptualization, M.G. and C.B.; Methodology, M.G., Y.K., D.H., S.H., and A.S.; Investigation, M.G., Y.K., F.K.G., T.N., S.H., and D.H.; Resources, D.H., S.H., A.S., J.K., and Janine Meyer; Writing – Original Draft, M.G., Y.K., and A.S.; Writing – Review & Editing, M.G., Y.K., M.M., Johann Meyer, B.F., S.H., D.H., F.K.G., and J.K.; Visualization, M.G. and Y.K.; Supervision, M.G., Johann Meyer, M.M., and A.S.; Funding Acquisition, C.B., M.G., A.S., B.F., and D.H.

CONFLICTS OF INTEREST

The authors declare no competing interests.

ACKNOWLEDGMENTS

The authors thank Janne Bretsch, Girmay Asgedom, Daniel Brand, and Verena Labenski for technical support. We are indebted to Prof. Dr. Thomas J. Hope from Northwestern University, Chicago, IL, USA for providing the pRSV.Rev expression plasmid. This work was supported by grants from the German Research Foundation

(DFG: Collaborative Research Centers 738/3 [projects C4 and C9] and 841 [project SP2], and REBIRTH Cluster of Excellence [EXC 62/1]) and German Cancer Aid (111743).

REFERENCES

1. Barrangou, R., Fremaux, C., Deveau, H., Richards, M., Boyaval, P., Moineau, S., Romero, D.A., and Horvath, P. (2007). CRISPR provides acquired resistance against viruses in prokaryotes. Science *315*, 1709–1712.
2. Horvath, P., and Barrangou, R. (2010). CRISPR/Cas, the immune system of bacteria and archaea. Science *327*, 167–170.
3. Garneau, J.E., Dupuis, M.-È., Villion, M., Romero, D.A., Barrangou, R., Boyaval, P., Fremaux, C., Horvath, P., Magadán, A.H., and Moineau, S. (2010). The CRISPR/Cas bacterial immune system cleaves bacteriophage and plasmid DNA. Nature *468*, 67–71.
4. Deltcheva, E., Chylinski, K., Sharma, C.M., Gonzales, K., Chao, Y., Pirzada, Z.A., Eckert, M.R., Vogel, J., and Charpentier, E. (2011). CRISPR RNA maturation by trans-encoded small RNA and host factor RNase III. Nature *471*, 602–607.
5. Hsu, P.D., Lander, E.S., and Zhang, F. (2014). Development and applications of CRISPR-Cas9 for genome engineering. Cell *157*, 1262–1278.
6. Jinek, M., East, A., Cheng, A., Lin, S., Ma, E., and Doudna, J. (2013). RNA-programmed genome editing in human cells. eLife *2*, e00471.
7. Mali, P., Yang, L., Esvelt, K.M., Aach, J., Guell, M., DiCarlo, J.E., Norville, J.E., and Church, G.M. (2013). RNA-guided human genome engineering via Cas9. Science *339*, 823–826.
8. Osakabe, Y., Watanabe, T., Sugano, S.S., Ueta, R., Ishihara, R., Shinozaki, K., and Osakabe, K. (2016). Optimization of CRISPR/Cas9 genome editing to modify abiotic stress responses in plants. Sci. Rep. *6*, 26685.
9. Reider Apel, A., d'Espaux, L., Wehrs, M., Sachs, D., Li, R.A., Tong, G.J., Garber, M., Nnadi, O., Zhuang, W., Hillson, N.J., et al. (2017). A Cas9-based toolkit to program gene expression in *Saccharomyces cerevisiae*. Nucleic Acids Res. *45*, 496–508.
10. Jinek, M., Chylinski, K., Fonfara, I., Hauer, M., Doudna, J.A., and Charpentier, E. (2012). A programmable dual-RNA-guided DNA endonuclease in adaptive bacterial immunity. Science *337*, 816–821.
11. Branzei, D., and Foiani, M. (2008). Regulation of DNA repair throughout the cell cycle. Nat. Rev. Mol. Cell Biol. *9*, 297–308.
12. Cornu, T.I., Mussolino, C., and Cathomen, T. (2017). Refining strategies to translate genome editing to the clinic. Nat. Med. *23*, 415–423.
13. Fehse, B., and Abramowski-Mock, U. (2018). The time is ripe for somatic genome editing: NIH program to strengthen translation. Mol. Ther. *26*, 671–674.
14. Janbandhu, V.C., Moik, D., and Fässler, R. (2014). Cre recombinase induces DNA damage and tetraploidy in the absence of loxP sites. Cell Cycle *13*, 462–470.
15. Loonstra, A., Vooijs, M., Beverloo, H.B., Allak, B.A., van Drunen, E., Kanaar, R., Berns, A., and Jonkers, J. (2001). Growth inhibition and DNA damage induced by Cre recombinase in mammalian cells. Proc. Natl. Acad. Sci. USA *98*, 9209–9214.
16. Galla, M., Will, E., Kraunus, J., Chen, L., and Baum, C. (2004). Retroviral pseudotransduction for targeted cell manipulation. Mol. Cell *16*, 309–315.
17. Galla, M., Schambach, A., Falk, C.S., Maetzig, T., Kuehle, J., Lange, K., Zychlinski, D., Heinz, N., Brugman, M.H., Göhring, G., et al. (2011). Avoiding cytotoxicity of transposases by dose-controlled mRNA delivery. Nucleic Acids Res. *39*, 7147–7160.
18. Cornu, T.I., Thibodeau-Beganny, S., Guhl, E., Alwin, S., Eichtinger, M., Joung, J.K., and Cathomen, T. (2008). DNA-binding specificity is a major determinant of the activity and toxicity of zinc-finger nucleases. Mol. Ther. *16*, 352–358.
19. Szczepek, M., Brondani, V., Büchel, J., Serrano, L., Segal, D.J., and Cathomen, T. (2007). Structure-based redesign of the dimerization interface reduces the toxicity of zinc-finger nucleases. Nat. Biotechnol. *25*, 786–793.
20. Pattanayak, V., Ramirez, C.L., Joung, J.K., and Liu, D.R. (2011). Revealing off-target cleavage specificities of zinc-finger nucleases by *in vitro* selection. Nat. Methods *8*, 765–770.
21. Kim, S., Kim, D., Cho, S.W., Kim, J., and Kim, J.-S. (2014). Highly efficient RNA-guided genome editing in human cells via delivery of purified Cas9 ribonucleoproteins. Genome Res. *24*, 1012–1019.
22. Liang, X., Potter, J., Kumar, S., Zou, Y., Quintanilla, R., Sridharan, M., Carte, J., Chen, W., Roark, N., Ranganathan, S., et al. (2015). Rapid and highly efficient mammalian cell engineering via Cas9 protein transfection. J. Biotechnol. *208*, 44–53.
23. Choi, J.G., Dang, Y., Abraham, S., Ma, H., Zhang, J., Guo, H., Cai, Y., Mikkelsen, J.G., Wu, H., Shankar, P., and Manjunath, N. (2016). Lentivirus pre-packed with Cas9 protein for safer gene editing. Gene Ther. *23*, 627–633.
24. Mock, U., Machowicz, R., Hauber, I., Horn, S., Abramowski, P., Berdien, B., Hauber, J., and Fehse, B. (2015). mRNA transfection of a novel TAL effector nuclease (TALEN) facilitates efficient knockout of HIV co-receptor CCR5. Nucleic Acids Res. *43*, 5560–5571.
25. Hendel, A., Bak, R.O., Clark, J.T., Kennedy, A.B., Ryan, D.E., Roy, S., Steinfeld, I., Lunstad, B.D., Kaiser, R.J., Wilkens, A.B., et al. (2015). Chemically modified guide RNAs enhance CRISPR-Cas genome editing in human primary cells. Nat. Biotechnol. *33*, 985–989.
26. Schumann, K., Lin, S., Boyer, E., Simeonov, D.R., Subramaniam, M., Gate, R.E., Haliburton, G.E., Ye, C.J., Bluestone, J.A., Doudna, J.A., and Marson, A. (2015). Generation of knock-in primary human T cells using Cas9 ribonucleoproteins. Proc. Natl. Acad. Sci. USA *112*, 10437–10442.
27. Cho, S.W., Kim, S., Kim, J.M., and Kim, J.-S. (2013). Targeted genome engineering in human cells with the Cas9 RNA-guided endonuclease. Nat. Biotechnol. *31*, 230–232.
28. Chen, X., and Gonçalves, M.A.F.V. (2016). Engineered viruses as genome editing devices. Mol. Ther. *24*, 447–457.
29. Maggio, I., Holkers, M., Liu, J., Janssen, J.M., Chen, X., and Gonçalves, M.A.F.V. (2014). Adenoviral vector delivery of RNA-guided CRISPR/Cas9 nuclease complexes induces targeted mutagenesis in a diverse array of human cells. Sci. Rep. *4*, 5105.
30. Hung, S.S.C., Chrysostomou, V., Li, F., Lim, J.K.H., Wang, J.H., Powell, J.E., Tu, L., Daniszewski, M., Lo, C., Wong, R.C., et al. (2016). AAV-mediated CRISPR/Cas gene editing of retinal cells *in vivo*. Invest. Ophthalmol. Vis. Sci. *57*, 3470–3476.
31. Bouard, D., Alazard-Dany, D., and Cosset, F.-L. (2009). Viral vectors: from virology to transgene expression. Br. J. Pharmacol. *157*, 153–165.
32. Lee, C.S., Bishop, E.S., Zhang, R., Yu, X., Farina, E.M., Yan, S., Zhao, C., Zheng, Z., Shu, Y., Wu, X., et al. (2017). Adenovirus-mediated gene delivery: Potential applications for gene and cell-based therapies in the new era of personalized medicine. Genes Dis. *4*, 43–63.
33. Ortinski, P.I., O'Donovan, B., Dong, X., and Kantor, B. (2017). Integrase-deficient lentiviral vector as an all-in-one platform for highly efficient CRISPR/Cas9-mediated gene editing. Mol. Ther. Methods Clin. Dev. *5*, 153–164.
34. Lund, A.H., Duch, M., Lovmand, J., Jørgensen, P., and Pedersen, F.S. (1997). Complementation of a primer binding site-impaired murine leukemia virus-derived retroviral vector by a genetically engineered tRNA-like primer. J. Virol. *71*, 1191–1195.
35. Nightingale, S.J., Hollis, R.P., Pepper, K.A., Petersen, D., Yu, X.-J., Yang, C., Bahner, I., and Kohn, D.B. (2006). Transient gene expression by nonintegrating lentiviral vectors. Mol. Ther. *13*, 1121–1132.
36. Voelkel, C., Galla, M., Maetzig, T., Warlich, E., Kuehle, J., Zychlinski, D., Bode, J., Cantz, T., Schambach, A., and Baum, C. (2010). Protein transduction from retroviral Gag precursors. Proc. Natl. Acad. Sci. USA *107*, 7805–7810.
37. Gabriel, R., Lombardo, A., Arens, A., Miller, J.C., Genovese, P., Kaeppel, C., Nowrouzi, A., Bartholomae, C.C., Wang, J., Friedman, G., et al. (2011). An unbiased genome-wide analysis of zinc-finger nuclease specificity. Nat. Biotechnol. *29*, 816–823.
38. Voelkel, C., Galla, M., Dannhauser, P.N., Maetzig, T., Sodeik, B., Schambach, A., and Baum, C. (2012). Pseudotype-independent nonspecific uptake of gammaretroviral and lentiviral particles in human cells. Hum. Gene Ther. *23*, 274–286.
39. Hamann, M.V., Stanke, N., Müllers, E., Stirnnagel, K., Hütter, S., Artegiani, B., Bragado Alonso, S., Calegari, F., and Lindemann, D. (2014). Efficient transient genetic manipulation *in vitro* and *in vivo* by prototype foamy virus-mediated nonviral RNA transfer. Mol. Ther. *22*, 1460–1471.

40. Mock, U., Riecken, K., Berdien, B., Qasim, W., Chan, E., Cathomen, T., and Fehse, B. (2014). Novel lentiviral vectors with mutated reverse transcriptase for mRNA delivery of TALE nucleases. Sci. Rep. *4*, 6409.

41. Galla, M., Schambach, A., Towers, G.J., and Baum, C. (2008). Cellular restriction of retrovirus particle-mediated mRNA transfer. J. Virol. *82*, 3069–3077.

42. Hoffmann, D., Schott, J.W., Geis, F.K., Lange, L., Müller, F.-J., Lenz, D., Zychlinski, D., Steinemann, D., Morgan, M., Moritz, T., and Schambach, A. (2017). Detailed comparison of retroviral vectors and promoter configurations for stable and high transgene expression in human induced pluripotent stem cells. Gene Ther. *24*, 298–307.

43. Uhlenbeck, O.C., Carey, J., Romaniuk, P.J., Lowary, P.T., and Beckett, D. (1983). Interaction of R17 coat protein with its RNA binding site for translational repression. J. Biomol. Struct. Dyn. *1*, 539–552.

44. Romaniuk, P.J., Lowary, P., Wu, H.N., Stormo, G., and Uhlenbeck, O.C. (1987). RNA binding site of R17 coat protein. Biochemistry *26*, 1563–1568.

45. Ni, C.-Z., Syed, R., Kodandapani, R., Wickersham, J., Peabody, D.S., and Ely, K.R. (1995). Crystal structure of the MS2 coat protein dimer: implications for RNA binding and virus assembly. Structure *3*, 255–263.

46. Buxbaum, A.R., Haimovich, G., and Singer, R.H. (2015). In the right place at the right time: visualizing and understanding mRNA localization. Nat. Rev. Mol. Cell Biol. *16*, 95–109.

47. Prel, A., Caval, V., Gayon, R., Ravassard, P., Duthoit, C., Payen, E., Maouche-Chretien, L., Creneguy, A., Nguyen, T.H., Martin, N., et al. (2015). Highly efficient *in vitro* and *in vivo* delivery of functional RNAs using new versatile MS2-chimeric retrovirus-like particles. Mol. Ther. Methods Clin. Dev. *2*, 15039.

48. Hu, W.S., and Temin, H.M. (1990). Retroviral recombination and reverse transcription. Science *250*, 1227–1233.

49. Peabody, D.S., and Lim, F. (1996). Complementation of RNA binding site mutations in MS2 coat protein heterodimers. Nucleic Acids Res. *24*, 2352–2359.

50. Schambach, A., Galla, M., Maetzig, T., Loew, R., and Baum, C. (2007). Improving transcriptional termination of self-inactivating gamma-retroviral and lentiviral vectors. Mol. Ther. *15*, 1167–1173.

51. Higashimoto, T., Urbinati, F., Perumbeti, A., Jiang, G., Zarzuela, A., Chang, L.-J., Kohn, D.B., and Malik, P. (2007). The woodchuck hepatitis virus post-transcriptional regulatory element reduces readthrough transcription from retroviral vectors. Gene Ther. *14*, 1298–1304.

52. Hope, T. (2002). Improving the post-transcriptional aspects of lentiviral vectors. Curr. Top. Microbiol. Immunol. *261*, 179–189.

53. Keryer-Bibens, C., Barreau, C., and Osborne, H.B. (2008). Tethering of proteins to RNAs by bacteriophage proteins. Biol. Cell *100*, 125–138.

54. Konermann, S., Brigham, M.D., Trevino, A.E., Joung, J., Abudayyeh, O.O., Barcena, C., Hsu, P.D., Habib, N., Gootenberg, J.S., Nishimasu, H., et al. (2015). Genome-scale transcriptional activation by an engineered CRISPR-Cas9 complex. Nature *517*, 583–588.

55. Mali, P., Aach, J., Stranges, P.B., Esvelt, K.M., Moosburner, M., Kosuri, S., Yang, L., and Church, G.M. (2013). CAS9 transcriptional activators for target specificity screening and paired nickases for cooperative genome engineering. Nat. Biotechnol. *31*, 833–838.

56. Heckl, D., Kowalczyk, M.S., Yudovich, D., Belizaire, R., Puram, R.V., McConkey, M.E., Thielke, A., Aster, J.C., Regev, A., and Ebert, B.L. (2014). Generation of mouse models of myeloid malignancy with combinatorial genetic lesions using CRISPR-Cas9 genome editing. Nat. Biotechnol. *32*, 941–946.

57. Mussolino, C., Morbitzer, R., Lütge, F., Dannemann, N., Lahaye, T., and Cathomen, T. (2011). A novel TALE nuclease scaffold enables high genome editing activity in combination with low toxicity. Nucleic Acids Res. *39*, 9283–9293.

58. Chatterjee, S., Behnam Azad, B., and Nimmagadda, S. (2014). The intricate role of CXCR4 in cancer. Adv. Cancer Res. *124*, 31–82.

59. Guo, F., Wang, Y., Liu, J., Mok, S.C., Xue, F., and Zhang, W. (2016). CXCL12/CXCR4: a symbiotic bridge linking cancer cells and their stromal neighbors in oncogenic communication networks. Oncogene *35*, 816–826.

60. Deng, H., Liu, R., Ellmeier, W., Choe, S., Unutmaz, D., Burkhart, M., Di Marzio, P., Marmon, S., Sutton, R.E., Hill, C.M., et al. (1996). Identification of a major co-receptor for primary isolates of HIV-1. Nature *381*, 661–666.

61. Feng, Y., Broder, C.C., Kennedy, P.E., and Berger, E.A. (1996). HIV-1 entry cofactor: functional cDNA cloning of a seven-transmembrane, G protein-coupled receptor. Science *272*, 872–877.

62. Hou, P., Chen, S., Wang, S., Yu, X., Chen, Y., Jiang, M., Zhuang, K., Ho, W., Hou, W., Huang, J., and Guo, D. (2015). Genome editing of CXCR4 by CRISPR/cas9 confers cells resistant to HIV-1 infection. Sci. Rep. *5*, 15577.

63. Cong, L., Ran, F.A., Cox, D., Lin, S., Barretto, R., Habib, N., Hsu, P.D., Wu, X., Jiang, W., Marraffini, L.A., and Zhang, F. (2013). Multiplex genome engineering using CRISPR/Cas systems. Science *339*, 819–823.

64. Pattanayak, V., Lin, S., Guilinger, J.P., Ma, E., Doudna, J.A., and Liu, D.R. (2013). High-throughput profiling of off-target DNA cleavage reveals RNA-programmed Cas9 nuclease specificity. Nat. Biotechnol. *31*, 839–843.

65. Fu, Y., Foden, J.A., Khayter, C., Maeder, M.L., Reyon, D., Joung, J.K., and Sander, J.D. (2013). High-frequency off-target mutagenesis induced by CRISPR-Cas nucleases in human cells. Nat. Biotechnol. *31*, 822–826.

66. Ashley, D.J. (1969). The two "hit" and multiple "hit" theories of carcinogenesis. Br. J. Cancer *23*, 313–328.

67. Knudson, A.G., Jr. (1971). Mutation and cancer: statistical study of retinoblastoma. Proc. Natl. Acad. Sci. USA *68*, 820–823.

68. Kelley, M.L., Strezoska, Ž., He, K., Vermeulen, A., and Smith, Av. (2016). Versatility of chemically synthesized guide RNAs for CRISPR-Cas9 genome editing. J. Biotechnol. *233*, 74–83.

69. Linial, M.L., and Miller, A.D. (1990). Retroviral RNA packaging: sequence requirements and implications. Curr. Top. Microbiol. Immunol. *157*, 125–152.

70. Telesnitsky, A., and Wolin, S.L. (2016). The host RNAs in retroviral particles. Viruses *8*, 235.

71. Linde, M.E., Colquhoun, D.R., Ubaida Mohien, C., Kole, T., Aquino, V., Cotter, R., Edwards, N., Hildreth, J.E., and Graham, D.R. (2013). The conserved set of host proteins incorporated into HIV-1 virions suggests a common egress pathway in multiple cell types. J. Proteome Res. *12*, 2045–2054.

72. Ma, H., Tu, L.-C., Naseri, A., Huisman, M., Zhang, S., Grunwald, D., and Pederson, T. (2016). CRISPR-Cas9 nuclear dynamics and target recognition in living cells. J. Cell Biol. *214*, 529–537.

73. Platt, R.J., Chen, S., Zhou, Y., Yim, M.J., Swiech, L., Kempton, H.R., Dahlman, J.E., Parnas, O., Eisenhaure, T.M., Jovanovic, M., et al. (2014). CRISPR-Cas9 knockin mice for genome editing and cancer modeling. Cell *159*, 440–455.

74. Mao, Z., Bozzella, M., Seluanov, A., and Gorbunova, V. (2008). Comparison of nonhomologous end joining and homologous recombination in human cells. DNA Repair (Amst.) *7*, 1765–1771.

75. Maruyama, T., Dougan, S.K., Truttmann, M.C., Bilate, A.M., Ingram, J.R., and Ploegh, H.L. (2015). Increasing the efficiency of precise genome editing with CRISPR-Cas9 by inhibition of nonhomologous end joining. Nat. Biotechnol. *33*, 538–542.

76. Gutschner, T., Haemmerle, M., Genovese, G., Draetta, G.F., and Chin, L. (2016). Post-translational Regulation of Cas9 during G1 Enhances Homology-Directed Repair. Cell Rep. *14*, 1555–1566.

77. Lin, S., Staahl, B.T., Alla, R.K., and Doudna, J.A. (2014). Enhanced homology-directed human genome engineering by controlled timing of CRISPR/Cas9 delivery. eLife *3*, e04766.

78. Cho, S.W., Kim, S., Kim, Y., Kweon, J., Kim, H.S., Bae, S., and Kim, J.S. (2014). Analysis of off-target effects of CRISPR/Cas-derived RNA-guided endonucleases and nickases. Genome Res. *24*, 132–141.

79. Zeitelhofer, M., Vessey, J.P., Xie, Y., Tübing, F., Thomas, S., Kiebler, M., and Dahm, R. (2007). High-efficiency transfection of mammalian neurons via nucleofection. Nat. Protoc. *2*, 1692–1704.

80. Zuris, J.A., Thompson, D.B., Shu, Y., Guilinger, J.P., Bessen, J.L., Hu, J.H., Maeder, M.L., Joung, J.K., Chen, Z.Y., and Liu, D.R. (2015). Cationic lipid-mediated delivery of proteins enables efficient protein-based genome editing *in vitro* and *in vivo*. Nat. Biotechnol. *33*, 73–80.

81. Mo, D., Potter, B.A., Bertrand, C.A., Hildebrand, J.D., Bruns, J.R., and Weisz, O.A. (2010). Nucleofection disrupts tight junction fence function to alter membrane polarity of renal epithelial cells. Am. J. Physiol. Renal Physiol. *299*, F1178–F1184.

82. Mello de Queiroz, F., Sánchez, A., Agarwal, J.R., Stühmer, W., and Pardo, L.A. (2012). Nucleofection induces non-specific changes in the metabolic activity of transfected cells. Mol. Biol. Rep. *39*, 2187–2194.

83. Buchholz, C.J., Friedel, T., and Büning, H. (2015). Surface-engineered viral vectors for selective and cell type-specific gene delivery. Trends Biotechnol. *33*, 777–790.

84. Wang, X., Herzog, R.W., Byrne, B.J., Kumar, S.R.P., Zhou, Q., Buchholz, C.J., and Biswas, M. (2017). Immune modulatory cell therapy for hemophilia B based on CD20-targeted lentiviral gene transfer to primary B cells. Mol. Ther. Methods Clin. Dev. *5*, 76–82.

85. Bender, R.R., Muth, A., Schneider, I.C., Friedel, T., Hartmann, J., Plückthun, A., Maisner, A., and Buchholz, C.J. (2016). Receptor-targeted Nipah virus glycoproteins improve cell-type selective gene delivery and reveal a preference for membrane-proximal cell attachment. PLoS Pathog. *12*, e1005641.

86. Segura, M.M., Garnier, A., Di Falco, M.R., Whissell, G., Meneses-Acosta, A., Arcand, N., and Kamen, A. (2008). Identification of host proteins associated with retroviral vector particles by proteomic analysis of highly purified vector preparations. J. Virol. *82*, 1107–1117.

87. Geisberg, J.V., Moqtaderi, Z., Fan, X., Ozsolak, F., and Struhl, K. (2014). Global analysis of mRNA isoform half-lives reveals stabilizing and destabilizing elements in yeast. Cell *156*, 812–824.

88. Borodulina, O.R., and Kramerov, D.A. (2008). Transcripts synthesized by RNA polymerase III can be polyadenylated in an AAUAAA-dependent manner. RNA *14*, 1865–1873.

89. Shi, J., Zhou, J., Shah, V.B., Aiken, C., and Whitby, K. (2011). Small-molecule inhibition of human immunodeficiency virus type 1 infection by virus capsid destabilization. J. Virol. *85*, 542–549.

90. Galla, M., Schambach, A., and Baum, C. (2013). Retrovirus-based mRNA transfer for transient cell manipulation. Methods Mol. Biol. *969*, 139–161.

91. Schambach, A., Bohne, J., Chandra, S., Will, E., Margison, G.P., Williams, D.A., and Baum, C. (2006). Equal potency of gammaretroviral and lentiviral SIN vectors for expression of O6-methylguanine-DNA methyltransferase in hematopoietic cells. Mol. Ther. *13*, 391–400.

92. Yang, Y., Vanin, E.F., Whitt, M.A., Fornerod, M., Zwart, R., Schneiderman, R.D., Grosveld, G., and Nienhuis, A.W. (1995). Inducible, high-level production of infectious murine leukemia retroviral vector particles pseudotyped with vesicular stomatitis virus G envelope protein. Hum. Gene Ther. *6*, 1203–1213.

93. Weber, K., Bartsch, U., Stocking, C., and Fehse, B. (2008). A multicolor panel of novel lentiviral "gene ontology" (LeGO) vectors for functional gene analysis. Mol. Ther. *16*, 698–706.

94. Dull, T., Zufferey, R., Kelly, M., Mandel, R.J., Nguyen, M., Trono, D., and Naldini, L. (1998). A third-generation lentivirus vector with a conditional packaging system. J. Virol. *72*, 8463–8471.

95. Schmittgen, T.D., and Livak, K.J. (2008). Analyzing real-time PCR data by the comparative C(T) method. Nat. Protoc. *3*, 1101–1108.

96. Ran, F.A., Hsu, P.D., Wright, J., Agarwala, V., Scott, D.A., and Zhang, F. (2013). Genome engineering using the CRISPR-Cas9 system. Nat. Protoc. *8*, 2281–2308.